Development of Novel Glucocorticoids for Use in Antibody−Drug Conjugates for the Treatment of Inflammatory Diseases

Amy Han,* Olav Olsen, Christopher D'Souza, Jing Shan, Feng Zhao, Jean Yanolatos, Zaruhi Hovhannisyan, Sokol Haxhinasto, Frank Delfino, and William Olson

Read Online

ACCESS | Metrics & More | Article Recommendations | Supporting Information

ABSTRACT: Glucocorticoids (GCs) are widely used to treat a variety of autoimmune and inflammatory diseases; however, systemic delivery of GCs is associated with side effects that affect essentially every organ system, reflecting the nearly ubiquitous expression of the glucocorticoid receptor (GR). Targeted delivery of GCs to diseased tissues using antibody-glucocorticoid conjugates (GC-ADCs) offers a therapeutic alternative to overcome these adverse effects. Herein, we describe novel classes of GCs that exhibited greater potency than dexamethasone and budesonide, a 100-fold selectivity toward the GR over other nuclear receptors, and no *in vitro* safety liability in pharmacology assays (hERG, AMES) and that demonstrated a substantial reduction in tumor necrosis factor-α (TNF-α) release in mice challenged with lipopolysaccharide (LPS). The site-specific conjugated GC-ADCs via cathepsin-cleavable linkers were highly stable in plasma and specifically released GCs in antigen-positive cells, suggesting that these novel GCs can serve as ADC payloads to treat autoimmune and inflammatory diseases.
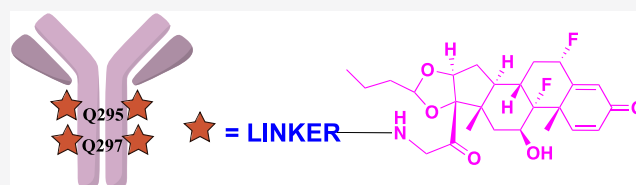
INTRODUCTION

Glucocorticoids (GCs) are an important therapeutic option for treating autoimmune and inflammatory disorders like asthma, rheumatoid arthritis, and inflammatory bowel disease.[1−3] The anti-inflammatory properties of GCs are attributed to their ability to bind to the GR and repress the expression of inflammatory genes. The downregulation of NF-κB, which promotes the expression of cytokines and adhesion proteins, is a major effector of the immunosuppressive effects of GCs.[4] However, because GCs regulate numerous other physiological functions, systemic administration of GCs is frequently limited due to serious adverse effects. To mitigate toxicities and widen the therapeutic window of GCs, alternative delivery methods such as topical, rectal, and inhalation have been employed with some success.[5] However, a safe, efficacious, systemically administered GC devoid of on-target, off-tissue toxicity remains elusive.

Antibody−drug conjugate (ADC) approaches have proven useful for delivering cytotoxic payloads to tumors. Ten ADCs are FDA-approved for the treatment of certain types of cancers, and at least eighty other ADCs are currently under clinical development. Targeting GCs using ADCs has the potential to improve the efficacy of GCs by expanding their therapeutic window while minimizing, or even eliminating, their adverse indications. Indeed, ABBV-3373, a GC-ADC based on adalimumab (Humira) targeting tumor necrosis factor for rheumatoid arthritis, entered clinical trials in 2019 in the treatment of patients with moderate-to-severe RA who had previously shown an inadequate response to methotrexate.[6]

ABBV-3373 displayed superior efficacy and safety as compared to adalimumab alone in a phase IIa clinical trial. Preclinically, fluticasone propionate was conjugated via its aliphatic hydroxyl group to an anti-CD74 antibody that targets antigen-presenting cells.[7] Budesonide was selectively delivered to immune cells via attachment to an anti-CD70 antibody.[8] Both examples utilized phosphate linkers that show significant hydrolysis in plasma at times (approximately 3 days) that are short compared to the circulating half-life of antibodies.[9] Recent references reported using nanobodies as vehicles for targeted delivery of payloads of interest, such as antigenic peptides (MOG) or small molecule (dexamethasone), which demonstrate the efficacy in prevention and treatment of experimental autoimmune encephalitis (EAE).[10]

We surmised that this concept could be extended to other GCs to provide a safe, potent, and effective means for the systemic administration of GCs. The payload used for modification in our study was budesonide, a potent GC with low oral bioavailability (%F = 9−20; controlled-release capsule) and extensive hepatic first-pass metabolism (∼90%). Budesonide is currently used for the treatment of inflammatory bowel disease, ulcerative colitis, and Crohn's disease. We
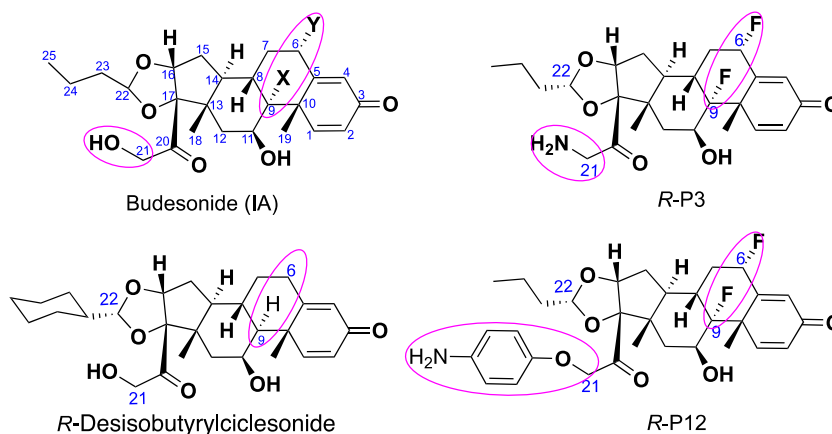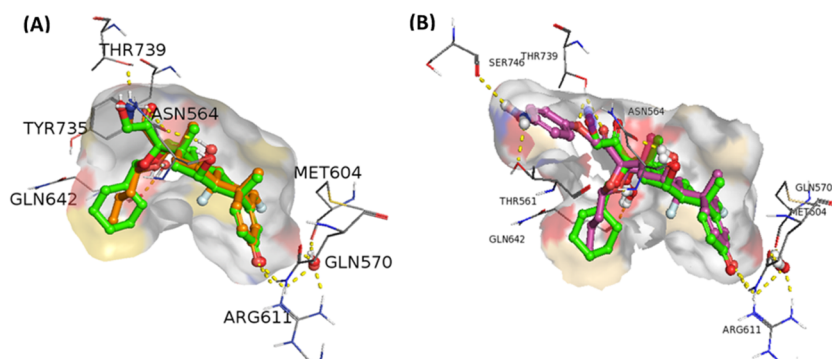
Figure 1. Budesonide analogue numbering system and regions focused on molecular modeling.

Figure 2. P3 (orange in 2A) and P12 (pink in 2B) docked in the binding pocket of crystal structure PDB-ID: 4UDD (*R*-desisobutyrylciclesonide in green and GR in gray) within the GR binding site. Both A&B were shown overlapping hydrogen bond interactions between the GR and the ligands: nitrogen atoms in blue, oxygen atoms in red, sulfur atoms in yellow, fluorine atoms in light blue, polar hydrogen atoms in white, and key hydrogen bonds in yellow dashed lines. 3D modeling results are available in separate supplemental PDB PYMOL files.

designed novel, potent, and selective budesonide derivatives and conjugated them to antibodies using linkers that are cleavable by cathepsin B and yet still stable in plasma. The ADCs were designed to deliver, and then release, the biologically active GC payloads to targeted cells, thereby potentially improving the therapeutic window and safety profile relative to nontargeted GCs.

RESULTS AND DISCUSSION

Our strategy for developing GC conjugates (GC-ADCs) began by identifying regions of budesonide that could be modified to improve the stability of the conjugate and potency of new free payloads. Two modifications of budesonide were evaluated: (1) replacement of the C^{21} hydroxyl group with amine or aniline group and (2) replacement of C^9 and C^6 hydrogen with fluorine. Amine- and aniline-containing payloads are routinely attached to antibodies via a carbamate linkage, which is expected to be more stable than a carbonate or phosphate linkage provided by hydroxyl groups.

Molecular Modeling Analysis of C^{21} Analogues. Molecular modeling of GC binding to the GR-active site was used to provide the rationale for C^{21} amine group substituents onto budesonide. Evaluation of PDB cocrystal structures, where ligands are complexed in the ligand-binding domain of the GR (residues 500−777), revealed desisobutyrylciclesonide complexed with GR (PDB code 4UDD).[11] In Figure 1, desisobutyrylciclesonide, a close structural homologue of budesonide, was used as a template to dock newly designed
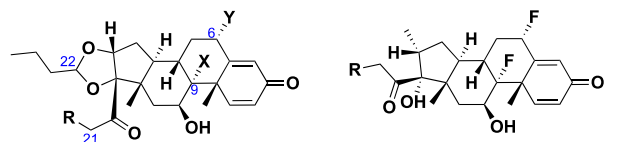
analogues (**P3** and **P12**) by employing the Schrödinger-induced fit docking program.

The optimal orientation of binding of **P3** and **P12** with the *R*-conformations is shown in Figure 2. *R*-**P3** (bound in the same orientation of desisobutyrylciclesonide) fits well in the active site of the GR (Figure 2A). The difference between *R*-**P3** and *R*-desisobutyrylciclesonide in the GR-active site is that the protonated amine group of *R*-**P3** interacts with the GR through hydrogen bonding with Thr739 and Asn564 and a cation−π interaction with Tyr735, while the C^{21}-hydroxy group of *R*-desisobutyrylciclesonide does not have a cation−π interaction with Tyr735. In addition, compared to *R*-desisobutyrylciclesonide, two fluorine atoms of *R*-**P3** fill the binding pocket more fully with the GR surface around *R*-desisobutyrylciclesonide. This observation may explain the different potencies observed between the GCs with and without fluorine at C^6 and C^9 and the general observation that fluorinate compounds are relatively more potent. The GR docking model of *R*-**P3** shows hydrogen bond interactions of the C^3 carbonyl group with Gln570 and Arg611, the C^{11} hydroxyl with Asn564, one oxygen atom (near C^{16}) of the dioxolane ring via a water molecule with Gln642, and the C^{21} protonated amine group with Thr739, Asn564. The molecular modeling of *R*-**P3** docked in the active site of the GR provided the foundation for the design and synthesis of new analogues. Figure 2B depicts the proposed binding mode of *R*-**P12** to the GR, which predicts a series of hydrogen bond networks between *R*-**P12** and the GR-active site. Key interactions

indicated are the C^{20} carbonyl interacting with Thr739 (Figure 2B). Interestingly, this interaction is not present in the C^{21} amine series for R-P3 (Figure 2A). Hydrogen bonding is also predicted between the ether oxygen at C^{21} of R-P12 and Thr739, as well as between the p-amino group of the phenoxy moiety with the hydroxyl side chain of Thr561 and the backbone carbonyl of Ser746. In addition, a water molecule mediates hydrogen bonding between an oxygen of the dioxolane ring (near C^{16}) and Gln642. Finally, hydrogen bonds of the C^3 carbonyl group with Gln570 and Arg611 and C^{11} hydroxyl with Asn564 also contribute to the binding of R-P12 within the active site of the GR. Taken together, molecular modeling studies of R-P3, R-P12, and the GR-active site suggest the formation of a complex network of hydrogen bonds that could translate into the discovery of novel potent glucocorticoids.

Synthesis of C^{21} Amino and Phenoxy Derivatives. The synthesis of C^{21} amine and C^{21} phenoxy derivatives of budesonide and its structurally similar glucocorticosteroid homologue, flumetasone, are listed in Table 1 and outlined in

Table 1. Structure−Activity Relationship (SAR) of C^{21} Amine and Phenoxy Derivatives of Budesonide and Flumetasone[a]

Budesonide analogues (P2-P6, P8-P13)   Flumetasone analogue (P7, P14)

	structures				cell-based EC$_{50}$	
cpd #	X	Y	R	cell-free GR binding IC$_{50}$	48 h	72 h
P1	H	H	OH	7.7/21.2*	3.3	3.1
R-**P1**	H	H	OH	7.2/11.3*	1.6	2.7
S-**P1**	H	H	OH	7.4/20.0*	12.0	22.0
P2	H	H	NH$_2$	NT/11.3*	13.0	16.4
P3	F	F	NH$_2$	NT/7.34*	1.17	1.59
R-**P3**	F	F	NH$_2$	1.90	0.90	1.47
S-**P3**	F	F	NH$_2$	13.2	6.26	11.2
P4	F	H	NH$_2$	NT	5.71	8.08
P5	F	F	NHMe	2.7	5.94	4.19
P6	F	F	NH-Ph-p-NH$_2$	3.7	1.31	1.42
P7	F	F	NH$_2$	38.7	>100	>100
R-**P8**	H	H	O-Ph-p-F	5.2	>100	>100
R-**P9**	H	H	O-Ph-p-NHAc	7.4	>100	>100
P10	H	H	O-Ph-p-NH$_2$	NT/2.6*	1.65	1.53
R-**P10**	H	H	O-Ph-p-NH$_2$	0.8	0.98	0.75
S-**P10**	H	H	O-Ph-p-NH$_2$	8.8	2.48	2.69
P11	F	F	O-Ph-m-NH$_2$	4.4	38.6	35.7
P12	F	F	O-Ph-p-NH$_2$	2.3	0.18	0.11
R-**P12**	F	F	O-Ph-p-NH$_2$	0.3	0.17	0.10
S-**P12**	F	F	O-Ph-p-NH$_2$	3.4	0.42	0.28
P13	F	F	O-Ph-p-CH$_2$NH$_2$	5.7	45.7	69.9
P14	F	F	O-Ph-p-NH$_2$	9.0	6.65	3.42

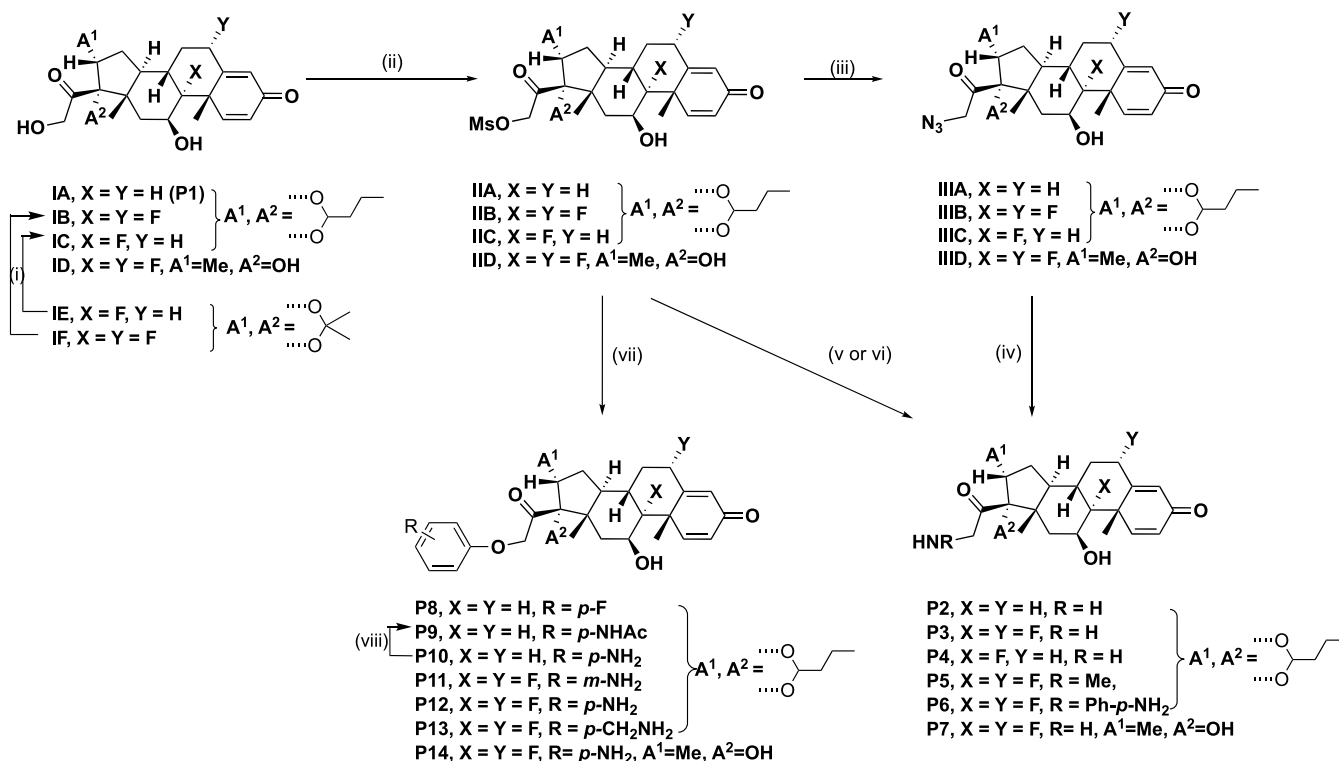[a]EC$_{50}$ values are mean values (n > 2) from HEK293/UAS-Luc/pBIND GR cell-based assay. IC$_{50}$ values are mean values (n > 2) in LanthaScreen time-resolved fluorescence resonance energy-transfer (TR-FRET) GR cell-free competition binding assay. *: Data were performed by Thermo Fisher, indicating that good binding activity is on the order of **P3** > **P2** > **P1** and **P10** > **P2**. NT, not tested. C^{22} epimer is the racemate; R- or S-epimer is a single chiral epimer at C^{22}.

Scheme 1. Detailed reaction conditions and yields are provided in the Experimental Section and/or Supporting Information section. In general, derivatives IA to IF were either synthesized according to known procedures or purchased commercially. C^{21} derivatives were derived as follows: budesonide (**P1**, IA), flumetasone (ID), triamcinolone acetonide (IE), and fluocinolone acetonide (IF) were commercially available. IB and IC were obtained from IE and IF, separately, by ketal exchange with butyraldehyde in the presence of perchloric acid (step i).[12] **P2** was derived from budesonide (IA); **P3**, **P5**, and **P6** from fluocinolone acetonide (IB); **P4** from triamcinolone acetonide (IC); and **P7** from ID. **P2**, **P3**, **P4**, and **P7** were obtained from a three-step process as follows. The C^{21} hydroxyl groups of IA to ID were first converted to their corresponding mesylates (IIA to IID, step ii),[13] which were then displaced by addition of sodium azide (IIIA to IIID, step iii) followed by subsequent reduction by triphenylphosphine (step iv). Alternatively, the mesylates (IIA and IIB) were directly converted to the corresponding amine derivative using ammonia in methanol (step v for **P2**) and aniline, which were derivatives produced using aniline reagents (step vi for **P6**), respectively. **P5** was obtained by converting the mesylate (IIB) to N-(p-methoxybenzyl)-**P5**, followed by deprotection with 1-chloroethyl carbonochloridate. Aniline derivatives (**P8**−**P14**) were prepared either via a one-step process, by displacing the mesylates with required phenols under basic conditions, or via a two-step process, by first reacting mesylates with substituted nitrophenols, followed by reduction of the nitro group to the desired amine group by employing iron dust and ammonium chloride (step vii). **P8**, **P10**, *S*-**P10**, and *R*-**P10** were obtained from IIA, **P11**, **P12**, *R*-**P12**, *S*-**P12**, and **P13** were obtained from IIB, and **P14** was obtained from IID. **P9** was obtained by exposure of **P10** to acetic anhydride (viii). All chiral R- and S-epimers were obtained either from using chiral reagents or from chiral supercritical fluid chromatography (SFC) or preparative high-performance liquid chromatography (HPLC) separations, as well characterized by chiral HPLC and ^{1}H NMR (see the Experimental Section and Supporting Information section). The identification of R- and S-C^{22} epimers was accomplished by observing van der Waals interactions (or lack thereof) between H^{16} and H^{22} in ^{1}H NMR spectra. Van der Waals interactions are observed between H^{16} and H^{22} in the S-epimer, where the chemical shift of H^{22} shifts downfield to ~5.23 ppm. For the R-epimer, H^{22} is more distal from H^{16} and no van der Waals interaction is observed; therefore, the chemical shift of H^{22} in the R-epimer is ~4.65 ppm.[14]

SAR of C^{21} Amino Derivatives. All designed analogues were tested in a cell-free TR-FRET GR competition binding assay (cell-free assay) and a cell-based GR coactivator luciferase reporter assay in HEK293/UAS-Luc/pBIND GR cells (cell-based assay). The bioassay results are listed in Table 1, and the assay details are given in the Supporting Information section. To compare the potency of the free GR agonists (payloads) to their corresponding ADCs (evaluated at the 3 day time point in cell-based assays), two time points (48 and 72 h) were chosen to measure the EC$_{50}$ of the free payloads in the cell-based assay. Cellular efflux rates were determined by Caco2 assay (see the Supporting Information).[15]

Budesonide (**P1**) demonstrated a mean IC$_{50}$ of 7.7 nM in the GR cell-free assay and activated the GR receptor with a mean EC$_{50}$ of 3.1 nM in the cell-based assay (72 h). Chiral separation of each C^{22} epimer of budesonide revealed that both

Scheme 1. Synthesis of C^{21} Amine and C^{21} Phenoxy Derivatives of Budesonide and Flumetasone[a]

IA, X = Y = H (P1)
IB, X = Y = F
IC, X = F, Y = H
ID, X = Y = F, A^1=Me, A^2=OH
$A^1, A^2 =$ ....O propyl

IE, X = F, Y = H
IF, X = Y = F
$A^1, A^2 =$ ....O isopropylidene

IIA, X = Y = H
IIB, X = Y = F
IIC, X = F, Y = H
IID, X = Y = F, A^1=Me, A^2=OH
$A^1, A^2 =$ ....O propyl

IIIA, X = Y = H
IIIB, X = Y = F
IIIC, X = F, Y = H
IIID, X = Y = F, A^1=Me, A^2=OH
$A^1, A^2 =$ ....O propyl

P8, X = Y = H, R = *p*-F
P9, X = Y = H, R = *p*-NHAc
P10, X = Y = H, R = *p*-NH$_2$
P11, X = Y = F, R = *m*-NH$_2$
P12, X = Y = F, R = *p*-NH$_2$
P13, X = Y = F, R = *p*-CH$_2$NH$_2$
P14, X = Y = F, R= *p*-NH$_2$, A^1=Me, A^2=OH
$A^1, A^2 =$ ....O propyl

P2, X = Y = H, R = H
P3, X = Y = F, R = H
P4, X = F, Y = H, R = H
P5, X = Y = F, R = Me,
P6, X = Y = F, R = Ph-*p*-NH$_2$
P7, X = Y = F, R= H, A^1=Me, A^2=OH
$A^1, A^2 =$ ....O propyl

[a](i) Butyraldehyde (1.5 equiv), HClO$_4$ (4.2 equiv), silica gel, heptanes, 10−20 °C, 18 h; (ii) CH$_3$SO$_2$Cl (1.5 equiv), 4-dimethylaminopyridine (DMAP) (2 equiv), pyridine, 0 °C; or for **IIB**: CH$_3$SO$_2$Cl (1.5 equiv), Et$_3$N (2 equiv), CH$_2$Cl$_2$, 0 °C, 30 min; (iii) NaN$_3$ (10 equiv), acetone, 50 °C, 18 h, (iv) PPh$_3$ (1.5 equiv), HCl (1 N) in tetrahydrofuran (THF), rt, 18 h; (v) for **P2**: NH$_3$ in CH$_3$OH (7 M), 40 °C, 18 h; (vi) for **P5** from **IIB**: PMB-NHCH$_3$, K$_2$CO$_3$ (3.0 equiv), CH$_3$CN, 70 °C, 5 h; then 1-chloroethyl carbonochloridate, chloroform, 70 °C, 1 h; for **P6** from **IIB**: 4-hydroxyaniline (5 equiv), Et$_3$N (10 equiv), NaI (3.7 equiv), *N,N*-dimethylformamide (DMF), 70 °C, 5 h; (vii) phenols or nitrophenols (2 equiv), Cs$_2$CO$_3$ or K$_2$CO$_3$, CH$_3$CN, 60−90 °C, 3 h; then for Boc-**P13**: trifluoroacetic acid (TFA)/CH$_2$Cl$_2$ and for nitro-precursors: Fe (10 equiv), NH$_4$Cl (11 equiv), EtOH/H$_2$O, 60−80 °C, 2 h, and (Viii) Ac$_2$O, CH$_2$Cl$_2$.

epimers exhibited equivalent GR binding, yet in the cell-based assay, the C^{22R} epimer (*R*-**P1**) displayed an ∼8-fold more potent agonist activity with an EC$_{50}$ of 2.7 nM than the C^{22S} epimer (*S*-**P1**) with an EC$_{50}$ of 22 nM.

Installation of the desired C^{21} amine group (**P2**) lowered the cellular functional activity by ∼5-fold relative to **P1**. The reduced cell-based activity of **P2** may be attributed to poorer A to B permeability resulting in a higher efflux ratio when compared to that of budesonide (1.19 for **P1** vs 4.94 for **P2**). Interestingly, insertion of a fluorine at C^9 (**P4**) increased cellular agonist activity by 2-fold relative to **P2**. Substitution of fluorine at both C^9 and C^6 of **P1** (**P3**) further improved cellular agonist activity (∼5-fold, EC$_{50}$: 1.59 nM) relative to **P4** and ∼10-fold relative to **P2**. Evaluation of the C^{22R}-epimer and C^{22S}-epimers of **P3** revealed that *R*-**P3** was ∼7-fold more potent than *S*-**P3** in cell-free assay (IC$_{50}$: 1.90 nM vs 13.2 nM, respectively) and 7.6-fold more potent than *S*-**P3** in the cell-based assay (EC$_{50}$ = 1.47 nM for *R*-**P3** vs EC$_{50}$ = 11.2 nM for *S*-**P3**). The improved binding results of *R*-/*S*-**P3** epimers relative to *R*-/*S*-**P1** epimers are likely from the larger size of fluorine, which our molecular model predicts may provide optimal space-filling over hydrogen (Figure 2A). These findings are consistent with a prior report that *R*-budesonide is more potent than its *S*-epimer[16] and are consistent with our finding (EC$_{50}$ = 2.7 nM for *R*-**P1** vs EC$_{50}$ = 22 nM for *S*-**P1**).

To probe the space available near the C^{21} amine group, *N*-methyl (**P5**) and *N*-phenyl-*p*-amino (**P6**) were installed off C^{21}

nitrogen. **P5** was shown to be less potent than **P3**, potentially due to loses of partial H-bonding network with C^{21} amine; however, **P6** preserved strong binding activity and cell-based activity as compared to **P3** (EC$_{50}$ = 1.59 nM for **P3** vs EC$_{50}$ =1.42 nM for **P6**), suggesting that phenyl substituents off the C^{21} amine are well tolerated. To evaluate whether substitution at the C^{22} dioxolane ring of the budesonide core could improve potency, an amine derivative of flumetasone, **P7**, was tested and found to be considerably less active than its budesonide analogue (**P3**, EC$_{50}$ = 1.59 nM vs >100 nM for **P7**) and also exhibited weak GR binding in the cell-free assay (IC$_{50}$: 38.7 nM), which may be due to the lack of a hydrogen binding network and/or higher efflux rate (8.57 for **P3** vs >16.2 for **P7**), indicating that the budesonide scaffold is preferred. In summary, insertion of an amine group at the C^{21} position of budesonide yields potent GR agonists that have the potential to serve as payloads for new ADCs.

SAR of C^{21} Phenoxy Derivatives. Molecular modeling predicts that replacing the C^{21} amine with a phenoxy (Figure 2B) may result in GR agonists with improved binding affinities. Indeed, inclusion of a *p*-aminophenoxy group at C^{21} (**P10**) improved activity in the cell-based activity, as well as the cell-free binding activity over **P1**, and showed similar potency to **P6** (Table 1). To evaluate the impact of the amino group for binding activity, the *p*-amino group of *R*-**P10** was replaced with a fluorine (*R*-**P8**) and protected to form the acetate (*R*-**P9**). Both *R*-**P8** and *R*-**P9** displayed a 10-fold loss of activity in the

cell-free binding assay, which correlates with our model predictions that a lack of H-bonding with the *p*-amino on phenyl group could result in reduced binding activity. Further, both compounds exhibited substantial loss of activity in the functional cell-based assay. Replacing C^9 and C^6 hydrogens with fluorine in **P10** provided **P12**, which was more potent than **P3** and budesonide (**P1**) in the cell-based assay (EC$_{50}$: 0.11 nM for **P12**) and also had a lower efflux rate compared to **P3** (8.57 for **P3** vs 0.86 for **P12**). Separation of the C^{22} epimers of **P12** revealed *R*-**P12** to be 10-fold more potent than *S*-**P12** in the cell-free binding assay (IC$_{50}$: 0.3 vs 3.4 nM) and ~3-fold more potent in the functional assay (EC$_{50}$: 0.1 vs 0.28 nM). Our findings regarding binding and cellular activity of *R*- and *S*-epimers of **P1**, **P3**, **P10**, and **P12** are consistent with earlier reports that C^{22R}-epimers of budesonide analogues are more potent than the C^{22S}-epimers.[16]

Based on the docking model of **P12** in the GR, the binding pocket was predicted to be encumbered for moving the *p*-amino group of **P12** to the meta position (**P11**) or changing the aromatic *p*-amino group to an aliphatic amine (**P13**) by extension of one carbon. **P11** exhibited reduced cellular functional activity >300-fold relative to **P12** (EC$_{50}$: 35.7 vs 0.11 nM); thus, the para-position of the amino group is desired. The activity of **P13** is reduced (IC$_{50}$ = 5.7 nM for **P13** vs IC$_{50}$ = 2.3 nM for **P12**) and its potency in the cell-based assay is impacted (EC$_{50}$ = 70 nM for **P13** vs EC$_{50}$ = 0.11 nM for **P12**). The lack of agonist activity in the cell-based assay with **P13** may also be attributed to its higher efflux rate (>18.9 for **P13** vs 0.86 for **P12**). To further evaluate whether substitution at the C^{22} dioxolane ring of budesonide could improve potency, the amino group of **P7** was replaced with *p*-aminophenoxy to form **P14**. Compared to the corresponding budesonide analogue **P12**, **P14** was 4-fold less potent in the GR binding assay and much less active than **P12** in the cell-based assay (EC$_{50}$= 3.4 nM for **P14** vs EC$_{50}$ = 0.11 nM for **P12**), presumably due to its higher efflux ratio (3.78 for **P14** vs 0.86 for **P12**).

In summary, C^{21} amine-containing substituents are well tolerated in the GR-active site and can produce more potent GR agonists than budesonide, as assessed by *in vitro* GR binding and cell-based GR activation assays. Budesonide (**P1**), **P3**, and **P12** were further evaluated in cell-free competition binding assays against a panel of 20 related nuclear receptors and showed IC$_{50}$ values >1000 nM against all other nuclear receptors tested except for the progesterone receptor (PR). Budesonide (**P1**) and **P3** showed comparable activity against GR and PR in cell-free assays (see the Supporting Information section). From these SAR analyses, **P3** and **P12** were chosen for further evaluation in absorption, distribution, metabolism, and excretion (ADME), *in vitro* safety, and *in vivo* PK studies to confirm the molecules as optimal payloads for the ADC approach to inflammatory and autoimmune diseases.

***In Vitro* Plasma Stability and *In Vivo* Pharmacokinetic Study.** **P3** and **P12** were evaluated for stability in mouse and human plasma.[17] **P3** exhibited excellent stability in both human ($T_{1/2}$ = 38.8 h) and mouse ($T_{1/2}$ = 4.3 h) plasma and **P12** had good stability in human ($T_{1/2}$ = 7.68 h) and mouse ($T_{1/2}$ = 2.74 h) plasma. Pharmacokinetic data were obtained for dexamethasone (Dex), **P3** and **P12**, at 1 mg/kg intraperitoneal (IP) dosing (*n* = 4 per group in male C57/6j mice). Mean blood concentration−time profiles of all three compounds are shown in Figure 3, and the PK parameters are summarized in Table 2. All three compounds were formulated
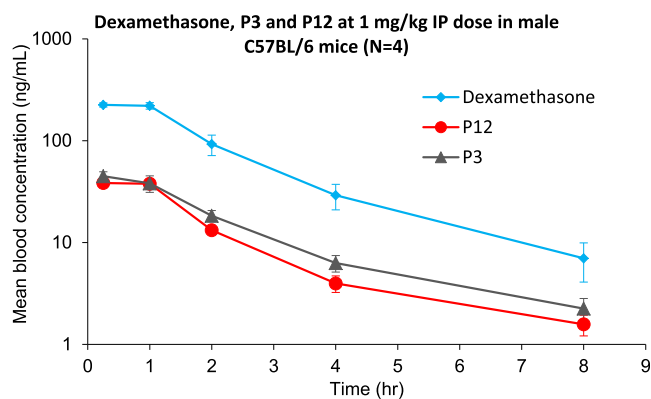
Figure 3. Pharmacokinetic graphs of dexamethasones **P3** and **P12**.

using 5% dimethyl sulfoxide (DMSO)/5% Tween-80/20% PEG400/70% saline for IP administration. Dex was evaluated because it was later included as a positive control in the *in vivo* LPS challenge study. **P3** and **P12** exhibited exposure levels (AUC) 5-6x lower than Dex but had comparable terminal $T_{1/2}$ values (1.6−1.9 h), as compared to Dex. No signs of overt toxicity were observed for any compound.

***In Vivo* LPS-Induced TNF-*α* Challenge.** Pharmacodynamic data for **P3** and **P12** are shown in Figure 4. **P3** and **P12** were evaluated in the endotoxin lipopolysaccharide (LPS)-induced proinflammatory cytokine tumor necrosis factor *α* (TNF-*α*) mouse model in Figure 4.[18] **P3** and **P12**, phosphate-buffered saline (PBS, pH 7.4, control), and Dex (positive control) were administered IP to C57BL/6j male mice (*n* = 4 per group) 2 h prior to IP dosing of LPS at 0.5 mg/Kg, which was considered time zero. At the 2 h post LPS dose, blood was drawn from the mice and TNF-*α* levels were measured by the enzyme-linked immunosorbent assay (ELISA). **P12** was also administered 24 and 48 h predose of LPS, separately, and TNF-*α* levels were measured 2 h postdose of LPS. As shown in Figure 4, Dex administration reduced TNF-*α* levels by 50%, while **P3** and **P12** reduced TNF-*α* levels by ~85%. Inhibition of TNF-*α* release by **P12** was time-dependent and inversely related to its time of dosing; **P12** inhibited TNF-*α* release by >50% even 24 h after dosing.

***In Vitro* Cardiotoxicity and Genotoxicity.** **P3** and **P12** were evaluated for their potential to have cardiotoxic effects caused by QT prolongation via inhibition of the hERG current. Using the patch-clamp technique,[19] both compounds exhibited no hERG inhibition (<2%; IC$_{50}$ > 30 *μ*M), indicating potentially no cardiotoxicity. To examine their mutagenesis potential, **P3** and **P12** were subjected to the mini-Ames genotoxicity assay.[20] TA98 (frameshift mutation) and TA100 (base-pair substitution) are two common strains of *Salmonella typhimurium* assessed in Ames testing. In both strains, the compounds did not induce a ≥2-fold increase in colony formation in the presence or absence of rat liver fractions (+/− S9), in concentrations up to 30 *μ*M indicating no evidence for mutagenic activity.

Synthesis of Linker−Payloads (LPs). **P3** and **P12** were attached to a cleavable ADC linker via a carbamate linkage to evaluate the stability and rate of release of the payload upon exposure to cathepsin B (CapB). The DIBAC-suc-PEG$_4$-vcPAB linker was chosen because the vcPAB moiety is controllably cleaved in the presence of CapB, a lysosomal cysteine protease.[21,22] Synthesis of linker−payloads (**LP1** and **LP2**, Table 3) was accomplished according to Scheme 2. **LP1**

Table 2. Pharmacokinetic Data of Dexamethasones P3 and P12[a]

PK parameters	units	dexamethasone			P3			P12		
		mean	SD	CV (%)	mean	SD	CV (%)	mean	SD	CV (%)
T_{max}	h	0.625	0.433	69.3	0.25	0	0	0.438	0.375	85.7
C_{max}	ng/mL	231	7.97	3.45	44.8	4.77	10.6	39.4	1.75	4.43
terminal $T_{1/2}$	h	1.64	0.187	11.4	1.91	0.21	11	1.69	0.62	36.7
AUC_{last}	h*ng/mL	545	60.6	11.1	107	13.6	12.7	84.6	7.71	9.12
AUC_{INF}	h*ng/mL	562	67.2	11.9	113	14.1	12.5	89.2	8.2	9.19

[a]The definitions of the pharmacokinetics symbols can be found at https://static.springer.com/sgw/documents/1372030/application/pdf/40262_cpk_symbols.pdf.
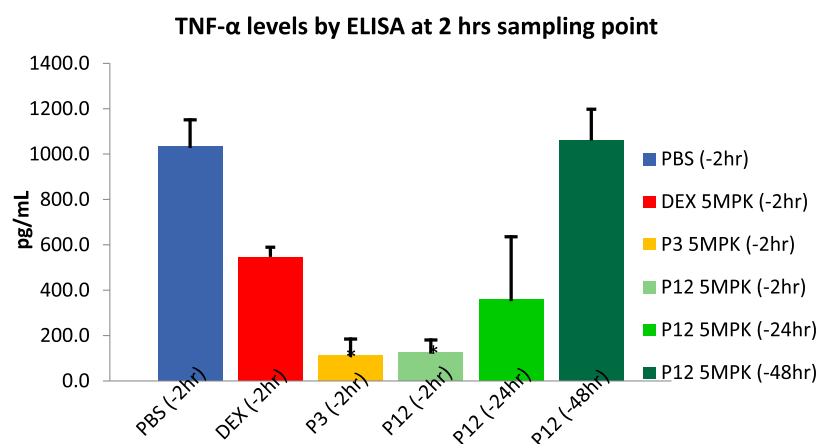

Figure 4. TNF-α levels following LPS administration to mice treated with PBS, Dex, **P3**, or **P12**.

Table 3. Structures of the Linker−Payloads (LPs) and Quenched Linker−Payloads (q-LPs); the Structures of Payloads Are Shown in Pink, and the Cleavable Linker Is Shown in Blue

LP# / Associated P#	Structure
LP1 / P3	
LP2 / P12	
Quenched q-LP1 / P3	
Quenched q-LP2 / P12	

is DIBAC-suc-PEG$_4$-vcPAB-**P3** and **LP2** is DIBAC-suc-PEG$_4$-vcPAB-**P12**. The reactions of payload-amine (**P3**) or payload-aniline (**P12**) with *N*-Fmoc protected Val-Cit-PAB-PNP (**IV**), followed by deprotection of *N*-Fmoc, generated the carbamates (**VA** and **VB**). Amide coupling of the amine (**VA** or **VB**) with DIBAC-suc-PEG$_4$-carboxylic acid (**VI**) formed the linker−

payloads, **LP1** or **LP2**, respectively. Due to poor aqueous solubility of the linker−payloads (**LP1** and **LP2**) in CapB assay media (<0.1 mg/mL), **LP1** and **LP2** were quenched with the highly water-soluble azido−PEG$_4$−SO$_3$H (**VIII**) via a [3+2] cycloaddition between the DIBAC moiety in **LP1** and **LP2** with the azido-moiety in **VIII** to generate the aqueously soluble

Scheme 2. Synthetic Route for Linker−Payloads (LP1 and LP2) and Their Corresponding Quenched Linker−Payloads (q-LP1 and q-LP2)[a]
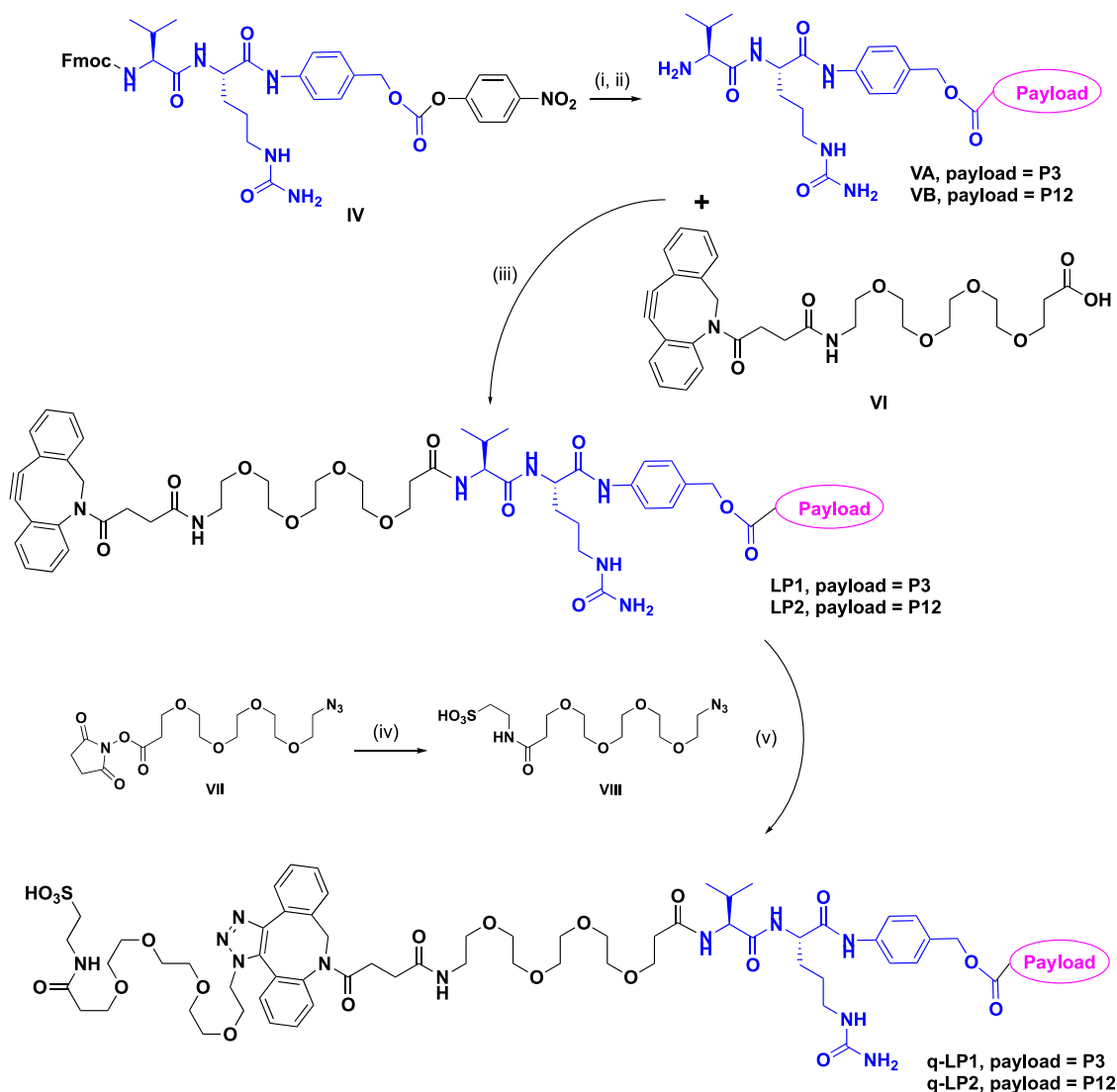
[a](i) payload; HOBt, N,N-diisopropylethylamine (DIEA), DMF, rt, 3 h; (ii) 20% piperidine, DMF, (iii) HATU, DIEA, DMF; (iv) DIEA, DMF, rt, 14 h; (v) CH$_3$CN/H$_2$O, rt, 14 h.

quenched linker−payloads (q-**LP1** and q-**LP2**), which were highly soluble (>0.5 mg/mL) in water and used in the CapB cleavage studies.

Cathepsin B (CapB) Cleavage of Linker−Payloads. The VC-linker was designed to be cleaved by CapB. Quenched linker−payloads (q-**LP1** and q-**LP2**) at an initial concentration of 25 μM were incubated in CapB with and without CapB inhibitor (CA074) for 4 h, separately. Both the quenched linker−payload and free payloads were evaluated using liquid chromatography-mass spectrometry (LC-MC)/MS, and the results are shown in Table 4. In the presence of CapB, **q-LP1** released 72% of payload **P3** and **q-LP2** released 35% of payload **P12**. In the presence of CapB and CA074, no payloads were released. Efficient release of the free payloads (**P3** and **P12**) from their corresponding linker−payload systems was demonstrated, thus warranting their further evaluation in ADC-conjugated systems. In this study, **LP1** exhibited a better cleavable rate over **LP2** and was more water-soluble over **LP2**.

Table 4. Analysis of Payloads Releasing from Quenched Linker−Payloads (q-LP1 and q-LP2) upon Exposure to Cathepsin B with and without CapB Inhibitor (CA074) at 4 h

sample	incubate with or without CA074	% remaining at 4 h	releasing payload		
			payload#	μM	conversion rate (%)
quenched LP1	without	<0.25	**P3**	18.05	**72.2**
	with	90.7		<1.00	<1.00
quenched LP2	without	3.65	**P12**	8.71	**34.8**
	with	82.12		<0.25	<1.0

Site-Specific Antibody−Drug Conjugations. Several organizations reported that microbial transglutaminase (mTG) was used to efficiently conjugate primary amine-based substrates to deglycosylated (Q295) or aglycosylated (N297Q) antibodies.[27] MTG is promiscuous with respect to

Scheme 3. Conjugation Process for GC-ADCs[a]
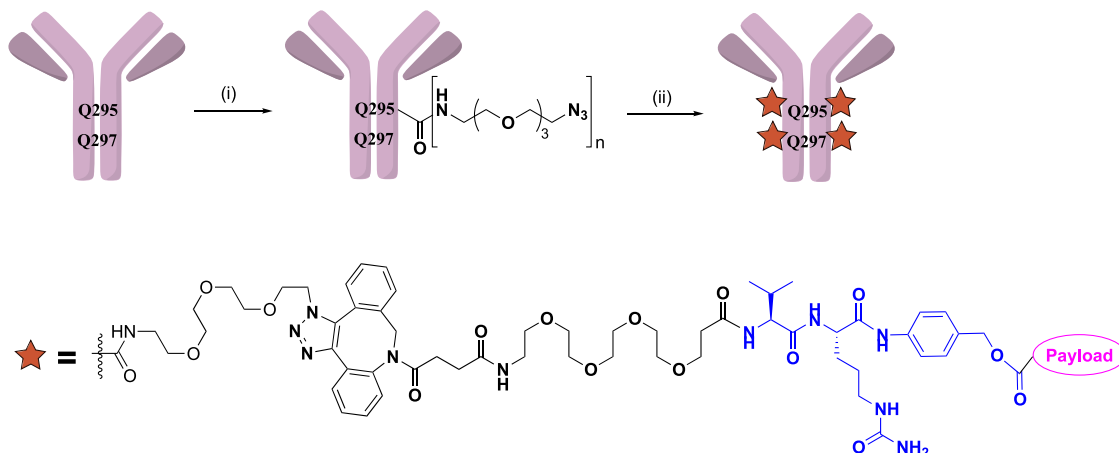
[a](i) MTG (25 U/mL; 5U MTG per mg of antibody), azido-dPEG$_3$-amine (≥200 equiv), pH 7−7.4; 37 °C, 4−24 h; and (ii) linker−payload (≥6 equiv), PBS, 5% glycerol, pH 7.4, 6−24 h.
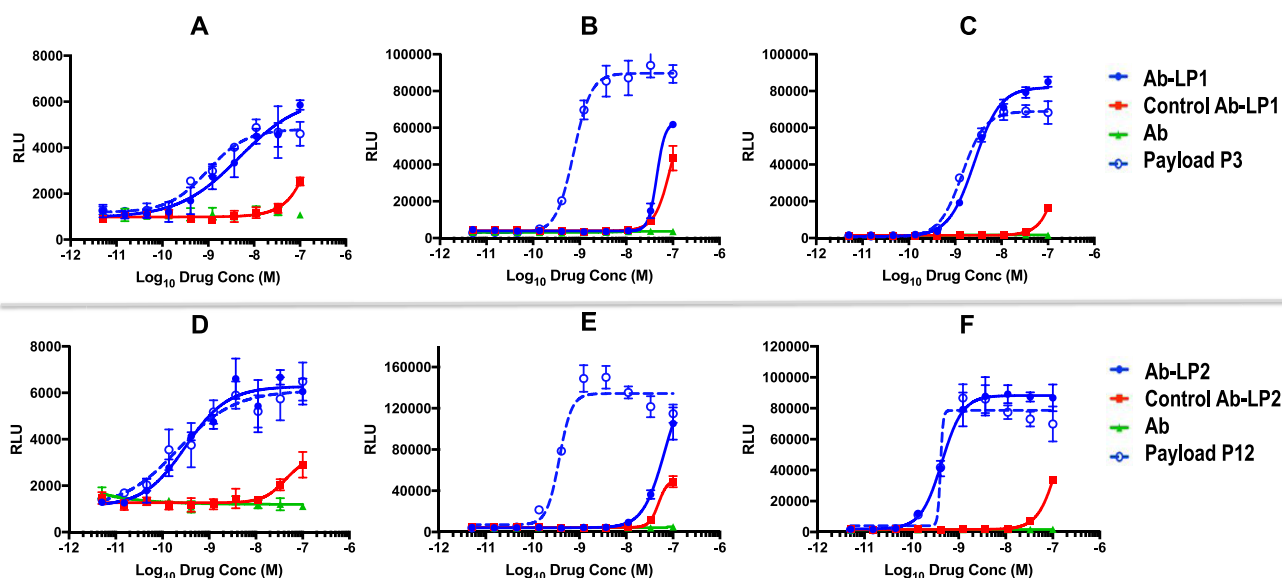
Test item	EC$_{50}$ (nM) in GR-Luc/PRLR (**A&D**)	EC$_{50}$ (nM) in GR-Luc (**B&E**)	EC$_{50}$ (nM) in 1:1 mixed GR-Luc with PRLR cells (**C&F**)
Anti PRLR-Ab-**LP1**	4.79	>45	2.61
Anti-Fel D1 Ab-**LP1**	>100	>93	>100
Free Payload of **LP1** (**P3**)	0.97	0.74	1.41
Anti PRLR-Ab-**LP2**	0.31	>67	0.44
Anti-Fel D1 Ab-**LP2**	>42	>49	>100
Free Payload of **LP2** (**P12**)	0.22	0.37	0.41
Unconjugated Anti PRLR-Ab	NA	NA	NA

Figure 5. Cell-based activities of anti-PRLR GC-ADCs, free payloads, and unconjugated anti-PRLR antibody in (1) A&D, GR-Luc/PRLR cells with antigen PRLR expression and GR luciferase reporter; (2) B&E, GR-Luc cells without PRLR expression; (3) PRLR cells without luciferase reporter (all compounds inactive; data not shown); and (4) C&F, mixture of cells (2) and (3) in a 1:1 ratio.

amine-based substrates but has a more restricted recognition of antibody Q295 and/or Q297-site and catalyzes the site-specific antibody−drug conjugations via formation of an isopeptide bond between the amines and the γ-carboxamide on the antibody-Q-site. Site-specific conjugations were performed using N297Q-mutated antibodies according to Scheme 3.[23]

A well-characterized aglycosylated anti-PRLR antibody (anti-PRLR Ab), which has been confirmed to be rapidly internalized into PRLR-expressing cells and deliver ADC payloads,[24] was selected for the conjugations. A cat allergen, Fel D1 antibody[25] (anti-Fel D1 Ab), was used as an isotype control antibody. The conjugation process involves two steps. The first step is microbial transglutaminase (MTG)-mediated attachment of a small molecular azide−PEG$_3$−amine (NH$_2$−PEG$_3$−N$_3$) to the antibodies, wherein an excess of the amine reagent was used to avoid potential cross-linking of antibody chains. The antibody was mixed with a solution of NH$_2$−PEG$_3$−N$_3$ (200 mol equiv to the antibody) in BupH, and the resulting solution was adjusted to pH 7.0−7.4 before mixing with transglutaminase (25 U/mL; 5U MTG per mg of antibody). The reaction mixture was then incubated at 37 °C for 4−24 h with gentle shaking, and the reaction progress was monitored by electrospray ionization (ESI)-MS. Upon completion of the reaction, the excess amine reagent and MTG were removed by size exclusion chromatography (SEC) to generate the antibody−azide conjugate (Ab−N$_3$). Addition of NH$_2$−PEG$_3$−N$_3$ at Q295 and Q297 on the two heavy chains of the N297Q-mutated antibody resulted in a four N$_3$-tagged conjugate (Ab−N$_3$). The conjugation sites were identified and confirmed by EEQ^{Linker}YQ^{Linker}STYR via peptide sequence mapping of trypsin-digested heavy chains of Ab−N$_3$. The second step attached the DIBAC-linked payload (LP) to the N$_3$-tagged conjugate (Ab−N$_3$) via a strain-promoted azide−alkyne cycloaddition (SPAAC). The conjugate mixtures were purified by SEC to generate the ADCs in up to 90% recovery yields. The ESI-MS results of the Ab−N$_3$ reagents showed 4×201 Da increasing from their corresponding anti-PRLR Ab and anti-Fel D1 Ab, indicating that both Q295 and Q297 on the antibodies were conjugated with the amine reagent. All mass additions of LP1 or LP2 to their corresponding Ab−N$_3$ were also confirmed by intact ESI-MS. The results indicated that the two-step conjugation/click reaction provided site-specific conjugates (ADCs) with approximately four linker−payloads per antibody (4DAR ADC) in up to 90% isolated yields when >6 molar equivalents of the linker−payload (LP1 or LP2) was used.

Antibody-Glucocorticoid (GC) Conjugate Cell-Based Activity and Bystander Effect. The activity of anti-PRLR antibody GC conjugates (anti-PRLR GC-ADCs) was evaluated side by side with their corresponding control anti-Fel D1 Ab GC conjugates (control GC-ADCs), free payloads (P3 and P12), and unconjugated anti-PRLR antibody (Ab) from serial dilutions at concentrations of 5.1−100 nM after 72 h of incubation in four types of cells: (1) HEK293/UAS-Luc/pBIND GR/PRLR cells are antigen-positive cells with GR reporter, aka GR-Luc/PRLR cells; (2) HEK293/UAS-Luc/pBIND GR cells are antigen-negative cells with GR reporter, aka GR-Luc cells; (3) HEK293/PRLR cells are antigen-positive cells devoid of a luciferase reporter, aka PRLR cells; and (4) mixture of cells (2) and (3) in 1:1 ratio. The results are shown in Figure 5A−F, with the free payloads shown in dotted blue lines, the anti-PRLR GC-ADCs shown in solid blue lines, control ADCs shown in red lines, and unconjugated anti-PRLR antibody shown in green lines.

The potency of an ADC was compared to its free payload based on molar concentrations of the free payload. The ADC concentration was normalized to the free payload concentration based on the ADC−DAR value. For example, for an ADC with a DAR of 4 (one antibody carries four drugs), the normalized ADC concentration is 4× its measured ADC concentration by UV at 280 nm. This is comparable to the free drug concentration if the payload is efficiently released from the ADC in the cell-based assay. In PRLR-expressing cells containing a GR reporter (Figure 5A), the free payload (P3; EC$_{50}$: 0.97) is more potent than the anti-PRLR Ab-LP1 conjugate, which had an EC$_{50}$ of 4.79 nM and showed greater than 100-fold selectivity over its control Ab-LP1 (EC$_{50}$ > 42 nM) and unconjugated Ab. In non-PRLR-expressing cells with a GR reporter (Figure 5B), only free payload P3 exhibited potent activity (EC$_{50}$: 0.74 nM). In mixed cell lines of (2) and (3) (Figure 5C), both free payload P3 (EC$_{50}$: 1.4 nM) and anti-PRLR Ab-LP1 (EC$_{50}$: 2.6 nM) demonstrated similar activity, whereas the control Ab-LP1 showed no activity (EC$_{50}$ > 100 nM). These results indicate that the anti-PRLR Ab-LP1 exhibits a bystander effect that involves the release of payload in the PRLR-expressing cell and then diffusion of the payload into neighboring cells. Similarly, in cells with the GR reporter and PRLR expression on the cell surface (Figure 5D), anti-PRLR Ab-LP2 (EC$_{50}$: 0.31 nM) demonstrated comparable potency to its free payload P12 (EC$_{50}$: 0.22 nM) with greater than 1000-fold selectivity over its control-ADC (EC$_{50}$ > 100 nM). In cells with the GR reporter without PRLR expression on the cell surface (Figure 5E), free payload P12 exhibited potent activity (EC$_{50}$: 0.37 nM), whereas its conjugate did not. In the mixed cells (Figure 5F), potent activity was observed for both free payload P12 (EC$_{50}$: 0.41 nM) and anti-PRLR Ab-LP2 (EC$_{50}$: 0.44 nM) but not the control Ab-LP2 (EC$_{50}$ > 100 nM), which is consistent of a bystander effect for anti-PRLR Ab-LP2. As expected, no luciferase activity was observed for either free drugs or conjugates in the cells without the GR reporter, confirming that the assay results are GR-reporter-dependent. Moreover, a greater selectivity (>1000×) was observed for anti-PRLR Ab-LP2 over its control, anti-Fel D1 Ab-LP2, vs >100× selectivity for anti-PRLR Ab-LP1 over its control, anti-Fel D1 Ab-LP1. This observation is attributed to P12 being a more potent-free payload with a lower efflux rate than P3. In conclusion, the GC-ADCs demonstrated potent GR activation and greater than 100-fold selectivity over their isotype control GC-ADCs in antigen-positive cell lines. Both GC-ADCs exhibited a bystander effect in mixed antigen-positive and -negative cell lines.

DISCUSSION AND CONCLUSIONS

We have utilized the ADC concept to carry payloads that have the potential to be used for the treatment of inflammatory and autoimmune diseases. By conducting an SAR of the budesonide molecule and simultaneously utilizing molecular modeling to improve the binding activity of drug analogues, two lead compounds (P3 and P12) emerged. Both compounds exhibited a >100-fold selectivity toward the glucocorticoid receptor (GR) over other nuclear hormone receptors, had better or identical potency in cell-based assays as compared to budesonide, demonstrated in vitro safety (no cardiotoxicity in hERG and no genotoxicity in Ames), exhibited potency in a proinflammatory *in vivo* mouse model, and, when attached to an ADC linker, were sufficiently released in the presence of cathepsin B. The work herein demonstrates the potential for both compounds to be used in a targeted manner to deliver the GR agonists to the desired cells and exert bystander activity on neighboring nonantigen-expressed cells, thus localizing their biological action and potentially reducing any side effects that are caused by systemic exposure. Future work will involve the

development of novel GC-ADCs for the treatment of inflammatory and autoimmune diseases.

■ EXPERIMENTAL SECTION

Molecular Modeling Procedure. The binding modes of compounds R-**P3** and R-**P12** (Figure 1) with the GR were modeled using the Schrödinger Drug Discovery Suite 2017.[26] The compounds were prepared using LigPrep, and possible ionization states were generated at pH 7.0 ± 1.0. For R-**P3**, the configuration with the protonated amine group was selected. The cocrystal structure of the GR in complex with desisobutyrylciclesonide (PDB-ID: 4UDD) was used as the receptor structure and was prepared using Protein Preparation Wizard. During protein preparation, only waters 2044 and 2084 located in the binding site were kept, and all other water molecules were removed. R-**P3** and R-**P12** were docked to 4UDD using induced fit docking with the box centered to the centroid of the ligand in 4UDD.

Cell-Based Assays. A glucocorticoid receptor (GR) coactivator luciferase reporter cell-based assay was used to analyze the GR activation by the GCs as a function of time. The HEK293 cell line was cotransfected with a construct expressing a fusion protein of the GR ligand-binding domain and the yeast Gal4 DNA domain (pBind GR, Promega) and a luciferase expression plasmid with Gal4 binding sites in the promoter region (pGL4.35[luc2P/9XGAL4UAS/Hygro], Promega). This cell line was referred to as HEK293/UAS-Luc/pBIND GR cells, which were further engineered to express human full-length PRLR on the cell surface and were referred to as HEK293/UAS-Luc/pBIND GR/PRLR cells. In addition, HEK293 cells were engineered to express human full-length PRLR only as a control cell line and were referred to as HEK293/PRLR cells. In the assay, 20 000/well of GR reporter cells were seeded in 96-well plates (Corning) in 80 μL of Dulbecco's modified Eagle's medium (DMEM) supplemented with 10% FBS and penicillin/streptomycin (complete media) and grown overnight at 37 °C and 5% CO_2. For dose−response curves, serially diluted compounds (20 μL ADC or free drug) were added to the cells and incubated for 48−72 h at 37 °C. Luciferase activity was determined by the addition of One-Glo reagent (Promega), and relative light units (RLUs) were measured on a Victor luminometer (Perkin Elmer). The EC_{50} values were determined from a four-parameter logistic equation over a 10-point response curve using GraphPadPrism.

Synthesis of Analogues. Reagents and solvents were obtained from commercial sources such as Sinopharm Chemical Reagent Co. (SCRC), Sigma-Aldrich, Alfa Aesar, or other vendors, unless explicitly stated otherwise. ^{1}H NMR and other NMR spectra were recorded on a Bruker AVIII 400 or Bruker AVIII 500. The data were processed with Nuts software or MestReNova software, measuring proton shifts in parts per million (ppm) downfield from an internal standard tetramethyl silane. All reactions were monitored by thin-layer chromatography (TLC) and LC-MS whenever possible, and all purified compounds were ≥95% purity based on analytical HPLC. HPLC (methods A, B, acidic, and basic), chiral HPLC, and ESI-MS conditions are described in the Supporting Information section.

General Procedure for the Synthesis of Mesylates IB and IC (Step i in Scheme 1). To a solution of fluocinolone acetonide (IF, 2 mmol) in heptanes (90 mL) were added silica gel (18 g) and butyraldehyde (3 mmol) at 10 °C. The suspension was stirred at 10−20 °C for 10 min and then perchloric acid (8.3 mmol) was added dropwise at 0 °C, and the resulting mixture was stirred at 10−20 °C for 18 h. The reaction mixture was diluted with petroleum ether and quenched with sat. aq. sodium carbonate. The suspension was filtered, and the solid was washed with dichloromethane/methanol (v/v = 1). The combined filtrate was separated, and the organic layer was concentrated *in vacuo*. The residue was purified by flash chromatography (0−100% ethyl acetate in petroleum ether) to give **IB** as a white solid. ESI m/z: 467.1 (M + H)[+]. The product was further purified by prep-HPLC (method B) to give C^{22R}-epimer (R-**IB**, 39% yield) and C^{22S}-epimer (S-**IB**, 9% yield) as white solids.

Following the procedure above, **IC** was obtained from fluocinolone acetonide (**IE**) in an 85% yield.

General Procedure for the Synthesis of Mesylates IIA−D (Step ii in Scheme 1). To a solution of budesonide (**IA**), **IB**, **IC**, or flumetasone (**ID**) (1 equiv) in pyridine (10 mL/g of compound) were added 4-dimethylaminopyridine (2 equiv) and methanesulfonyl chloride (1.5 equiv) dropwise at 0 °C. After stirring at rt for 2 h, the mixture was poured into ethyl acetate. The mixture was washed with diluted aq. hydrochloride (1 N) and brine, dried over sodium sulfate, and concentrated. The crude product was purified by flash chromatography (0−2% methanol in dichloromethane) to provide mesylates **IIA−D**.

General Procedure for the Synthesis of the Glucocorticoid-Amines P3, P4, and P7 (Steps iii and iv in Scheme 1). A solution of **IIB**, **IIC**, or **IID** (1 equiv) and sodium azide (10 equiv) in acetone (15 mL/g of compound) was stirred at 50 °C for 18 h. After cooling to rt, the mixture was poured into cold water (1×) and extracted with ethyl acetate (3×). The combined organic fractions were washed with brine, dried over sodium sulfate, and concentrated *in vacuo* to afford the crude azide derivatives (**IIIA−D**) as yellow solids. To a solution of crude **IIIB**, **IIIC**, or **IIID** (1 mmol) in THF (20 mL) and HCl (1 N, 10 mL) at rt was added triphenylphosphine (2.6 mmol), and the resulting solution was stirred at rt for 18 h. The mixture was concentrated *in vacuo*, and the residue was purified by prep-HPLC (method A) to provide the TFA salt or by prep-HPLC (method B) to provide the free base of **P3**, **P4**, or **P7**.

Synthesis of Payload P2 (Step v in Scheme 1). A solution of **IIA** (0.10 g, 0.20 mmol) in ammonia in methanol (7 M, 15 mL) was stirred at 40 °C for 18 h. The reaction mixture was concentrated *in vacuo*, and the crude was purified by prep-HPLC (method B) to give **P2** (8 mg, 9% yield) as an off-white solid. ESI m/z: 429.9 (M + H)[+]; ^{1}H NMR (CD₃OD, 400 MHz) δ 7.46 (d, J = 10.0 Hz, 1H), 6.26 (d, J = 10.0 Hz, 1H), 6.02 (s, 1H), 5.22−5.15 (m, 1.5H), 4.58 (m, 0.5H), 4.42 (m, 1H), 3.96−3.81 (m, 1H), 3.50−3.41 (m, 1H), 2.70−2.63 (m, 1H), 2.40−2.37 (m, 1H), 2.22−1.94 (m, 3H), 1.87−1.25 (m, 11H), 1.17−0.80 (8H) ppm.; *anal.* HPLC: purity is >95%.

Synthesis of Payload P3 (Steps iii and iv in Scheme 1). Following general procedure for steps iii and iv, **P3** (0.56 g, 56% yield in two steps) was obtained as an off-white solid (TFA salt) from **IIB**. ESI m/z: 466 (M + H)[+]; ^{1}H NMR (400 MHz, DMSO-d_6) δ 8.14 (s, 3H), 7.31 (d, J = 10.2 Hz, 1H), 6.31 (dd, J = 10.1 Hz, 1.6 Hz, 1H), 6.11 (s, 1H), 5.71−5.54 (m, 1H), 5.22 (t, J = 4.8 Hz, 0.4H), 5.15 (d, J = 7.6 Hz, 0.4 H), 4.78 (m, 0.6H), 4.67 (t, J = 4.4 Hz, 0.6H), 4.20−4.18 (m, 2H), 3.77 (m, 1H), 2.67−2.50 (m, 1H), 2.28−2.26 (m, 1H), 2.09−2.01 (m, 2H), 1.87−1.79 (m, 1H), 1.68−1.56 (m, 5H), 1.48 (s, 3H), 1.44−1.31 (m, 2H), 0.87 (t, J = 7.2, 3H), 0.85 (s, 3H) ppm.; *anal.* HPLC: purity is 100%.

R-**P3** was obtained from R-**IIB** (30 mg, 66% yield in two steps) as a white solid TFA salt after purification by prep-HPLC (method A). ESI m/z: 466 (M + H)[+]; ^{1}H NMR (500 MHz, DMSO-d_6) δ 8.14 (s, 3H), 7.30 (d, J = 10.0 Hz, 1H), 6.31 (dd, J = 10.0 Hz, 1.6 Hz, 1H), 6.11 (s, 1H), 5.71−5.55 (m, 1H), 4.78 (m, 1H), 4.67 (t, J = 4.4 Hz, 1H), 4.22 (m, 1H), 4.20 (d, J = 19 Hz, 1H),, 3.77 (d, J = 19 Hz, 1H), 2.67−2.50 (m, 1H), 2.28−2.26 (m, 1H), 2.09−2.01 (m, 1H), 2.09−2.01 (m, 2H), 1.68−1.56 (m, 5H), 1.48 (s, 3H), 1.44−1.31 (m, 3H), 0.87 (t, J = 7.2 Hz, 3H), 0.85 (s, 3H) ppm.; *anal.* HPLC: purity is 100%.

S-**P3** was obtained from S-**IIB**.[1] ESI m/z: 466 (M + H); H NMR (400 MHz, DMSO-d_6) δ 8.12 (brs, 3H), 7.30 (d, J = 10.0 Hz, 1H), 6.30 (dd, J = 1.6 Hz, 10.0 Hz, 1H), 6.11 (s, 1H), 5.71−5.54 (m, 1H), 5.22 (t, J = 4.8 Hz, 1H), 5.15 (d, J = 7.6 Hz, 1H), 4.18 (m, 1H), 4.15 (d, J = 19 Hz, 1H), 3.74 (d, J = 19 Hz, 1H), 2.58−2.53 (m, 1H), 2.25−2.22 (m, 1H), 2.03−1.97 (m, 2H), 1.87−1.79 (m, 1H), 1.72−1.52 (m, 3H), 1.48 (m, 5H), 1.34−1.28 (m, 2H), 0.91 (s, 3H), 0.88 (t, J = 7.2 Hz, 3H).; *anal.* HPLC: purity is 100%.

Synthesis of Payload P4 (Steps iii and iv in Scheme 1). Following general procedure of steps iii and iv, **P4** (5 mg, 6% yield in two steps) was obtained from **IIC** in a 2:1 ratio of $C^{22R/S}$ epimers as a yellow solid TFA salt after prep-HPLC purification (method A). ESI m/z: 448 (M + H)[+]; ^{1}H NMR (500 MHz, d_6-DMSO) δ 8.04 (s, 3H),

7.95−7.70 (m, 1H), 7.32 (d, *J* = 10 Hz, 1H), 6.24 (d, *J* = 9.0 Hz, 1H), 6.02 (s, 1H), 5.65−5.55 (m, 1H), 5.18 (t, *J* = 4 Hz, 0.24H), 5.12 (d, *J* = 5 Hz, 0.24H), 4.77 (d, *J* = 5.0 Hz, 0.76H), 4.66 (t, *J* = 4 Hz, 0.76H), 4.25−4.10 (m, 2H), 3.80−3.70 (m, 1H), 2.65−2.55 (m, 1H), 2.36−2.30 (m, 1H), 2.05−1.95 (m, 2H), 1.85−1.75 (m, 1H), 1.70−1.55 (m, 4H), 1.48 (s, 3H), 1.40−1.30 (m, 3H), 1.25−1.20 (m, 1H), 0.90−0.80 (m, 6H) ppm.

Synthesis of Payload P5 (Step vi in Scheme 1). To **IIB** (0.55 g, 1.0 mmol) in acetonitrile (10 mL) were added 4-(methoxybenzyl)-*N*-methylamine (0.30 g, 2.0 mmol) and potassium carbonate (0.41 g, 3.0 mmol). The mixture was refluxed (70 °C oil bath) for 5 h, cooled to rt, and then poured into water and extracted with ethyl acetate. The combined organic solution was dried over sodium sulfate and concentrated *in vacuo* to obtain 200 mg of residue. The residue (30 mg) was dissolved in chloroform (0.4 mL) and placed in a 4 mL screw-cap vial. To the solution was added 1 drop of 1-chloroethyl carbonochloridate, and the mixture was stirred at 70 °C in a sealed vial for 1 h. The volatiles were removed *in vacuo*, and the residue was purified by prep-HPLC (method A) to afford **P5** (8.0 mg, 9% yield in two steps) as a white solid. ESI *m/z*: 480 (M + H)⁺; ¹H NMR (400 MHz, CD₃OD) δ 7.34 (d, *J* = 10.1 Hz, 1H), 6.41−6.26 (m, 2H), 5.68−5.43 (m, 1H), 5.28 (t, *J* = 4.9 Hz, 0.75H), 5.23 (d, *J* = 7.4 Hz, 0.75H), 4.76 (m, 0.25H), 4.70 (m, 0.25H), 4.47−4.41 (m, 1H), 4.34−4.30 (m, 1H), 4.07−4.00 (m, 1H), 2.82−2.54 (m, 4H), 2.43−2.09 (m, 3H), 2.02−1.88 (m, 1H), 1.81−1.34 (m, 10H), 1.10−0.85 (m, 6H) ppm.; *anal.* HPLC: purity is 99%.

Synthesis of Payload P6 (Step vi in Scheme 1). To a solution of **IIB** (0.10 g, 0.18 mmol) in DMF (2 mL) in a screw-cap vial were added 4-hydroxyaniline (0.10 mg, 0.92 mmol), triethylamine (0.20 g, 2.0 mmol), and sodium iodide (0.10 g, 0.67 mmol). The mixture was stirred at 70 °C for 5 h and then cooled to rt. The reaction mixture was purified by prep-HPLC (method A) to give **P6** (10 mg, 8% yield) as a white solid. ESI *m/z*: 557 (M + H); ¹H NMR (500 MHz, *d₆*-DMSO) δ 9.59 (br s, 3H), 7.37 (d, *J* = 7.2 Hz, 0.1 H), 7.28 (d, *J* = 8.4 Hz, 0.9 H), 7.25 (d, *J* = 7.2 Hz, 0.1H), 7.07 (m, 1.8H), 6.81(m, 0.1H), 6.66−6.60 (m, 2H), 6.31 (dd, *J* = 8, 1.8 Hz, 1H), 6.12 (s, 1H), 5.68−5.57 (m, 1H), 5.54 (m, 1H), 5.25 (t, *J* = 9 Hz, 0.1H), 5.15 (d, *J* = 6 Hz, 0.1H), 4.80 (d, *J* = 3 Hz, 0.9H), 4.66 (t, *J* = 3.6 Hz, 0.9H), 4.36 (d, *J* = 16 Hz, 0.9H), 4.23 (m, 1.1H), 3.96 (d, *J* = 16 Hz, 0.9H), 3.87 (d, *J* = 16 Hz, 0.1H), 2.65−2.58 (m, 1H), 2.28 (m, 1H), 2.15−1.99 (m, 2H), 1.83−1.80 (m, 1H), 1.61−1.34 (m, 10H), 0.90−0.83 (m, 6H) ppm.; *anal.* HPLC: purity is >99%.

Synthesis of Payload P7 (Steps iii and iv in Scheme 1). Following general procedures of steps iii and iv, **P7** (0.18 g, 21% yield in two steps) is obtained as a white solid (TFA salt) from **IID**. ESI *m/z*: 410 (M + H)⁺; ¹H NMR (400 MHz, *d₆*-DMSO) δ 8.17 (s, 3H), 7.36 (d, *J* = 10.3 Hz, 1H), 6.29 (dd, *J* = 10.2, 1.7 Hz, 1H), 6.11 (s, 1H), 5.74−5.54 (m, 2H), 5.42 (s, 1H), 4.28−4.10 (m, 2H), 3.70−3.59 (m, 1H), 3.02−2.89 (m, 1H), 2.58−2.40 (m, 1H), 2.31−2.12 (m, 3H), 1.77−1.64 (m, 1H), 1.51−1.44 (m, 5H), 1.16−1.06 (m, 1H), 0.91 (s, 3H), 0.82 (d, *J* = 7.2 Hz, 3H).ppm.; *anal.* HPLC: purity is >99%.

General Procedure for Making Aniline Derivatives from Their Mesylates (Step vii in Scheme 1). To hot acetonitrile or acetone (60−90 °C) were added mesylates **IIB** or **IID** (1 equiv), corresponding phenol (2.0−2.5 equiv), and potassium carbonate or cesium carbonate (2.0−3.0 equiv). The resulting suspension was refluxed for 2−3 h, and then the volatiles were removed *in vacuo*. The residues were dissolved in water and ethyl acetate. The organic solution was separated and washed with water and brine, dried over sodium sulfate, and concentrated *in vacuo*. The crude products were purified by flash chromatography or prep-HPLC to give the desired phenoxy analogues. Reduction of nitro-substituted phenoxy analogues to the corresponding anilines is described as follows: to a suspension of iron powder (10 equiv) in ethanol (3 mL/g of iron) and water (0.75 mL/g of iron) were added the nitro-intermediate (1 equiv) and ammonium chloride (11 equiv). The resulting suspensions were stirred at 60−80 °C for 2 h and then cooled to rt, diluted with ethyl acetate, and filtered through celite. The filtrates were dried over sodium sulfate and concentrated *in vacuo*. The residues were purified by flash chromatography (30−70% ethyl acetate in petroleum ether)

or by prep-HPLC (method B) to provide the desired amines as free base or by prep-HPLC (method A) to provide TFA salts.

Synthesis of Payload P8 (Step vii in Scheme 1). Following general procedure of step vii, **P8** (14 mg, 54% yield) was obtained as a white solid after prep-HPLC (method B) from **IIA** (49 *μ*mol), 4-fluoro-phenol (0.18 mmol), and potassium carbonate (0.18 mmol) in acetone (1 mL). ESI *m/z*: 525 (M + H)⁺; ¹H NMR (400 MHz, CD₃OD) δ 7.47 (d, *J* = 10.1 Hz, 1H), 7.02 (t, *J* = 8.7 Hz, 2H), 6.94−6.90 (m, 2H), 6.27 (dd, *J* = 10.1, 1.8 Hz, 1H), 6.03 (s, 1H), 5.06 (d, *J* = 18.1 Hz, 1H), 4.90−4.88 (m, 1H), 4.82 (d, *J* = 18.1 Hz, 1H), 4.69 (t, *J* = 4.4 Hz, 1H), 4.46 (d, *J* = 2.8 Hz, 1H), 2.71−2.63 (m, 1H), 2.42−2.38 (m, 1H), 2.30−2.11 (m, 2H), 2.05−2.01 (m, 1H), 1.89−1.84 (m, 1H), 1.77−1.63 (m, 5H), 1.51−1.41 (m, 5H), 1.18−1.02 (m, 2H), 0.97−0.93 (m, 6H) ppm.; *anal.* HPLC: purity is 100%.

Synthesis of Payload P9 (Step viii in Scheme 1). To a solution of **P10** (50 mg, 96 *μ*mol) in CH₂Cl₂ (1 mL) was added acetic anhydride (0.25 mmol) via syringe at 0 °C. The resulting solution was stirred at 10−20 °C for 3 h. The reaction was quenched with methanol, and the mixture was concentrated *in vacuo*. The residue was purified by prep-HPLC (method B) to give **P9** (46% yield) as a white solid. ESI *m/z*: 564.3 (M + H)⁺; ¹H NMR (500 MHz, CD₃OD) δ 7.49−7.45 (m, 3H), 6.89 (d, *J* = 9.0 Hz, 2H), 6.28 (d, *J* = 10.2 Hz, 1H), 6.04 (s, 1H), 5.09 (d, *J* = 18.1 Hz, 1H), 4.91−4.89 (m, 1H), 4.83 (d, *J* = 18.1 Hz, 1H), 4.70 (t, *J* = 4.3 Hz, 1H), 4.47 (d, *J* = 3 Hz, 1H), 2.72−2.65 (m, 1H), 2.43−2.39 (m, 1H), 2.30−2.22 (m, 1H), 2.18−2.12 (m, 4H), 2.06−2.03 (m, 1H), 1.90−1.86 (m, 1H), 1.77−1.65 (m, 5H), 1.48 (m, 5H), 1.18−1.09 (m, 1H), 1.07−1.04 (m, 1H), 0.99−0.95 (m, 6H) ppm.; *anal.* HPLC: purity is 100%.

Synthesis of Payloads P10, S-P10, and R-P10 (Step vii in Scheme 1). Following general procedure of step vii, **P10** (50 mg, 50% yield) was obtained as a white solid from **IIB** (0.2 mmol), 4-nitrophenol (0.4 mmol), and cesium carbonate (0.4 mmol) in acetonitrile (5 mL). ESI *m/z*: 522 (M + H)⁺; ¹H NMR (500 MHz, CD₃OD) δ 7.47 (d, *J* = 10.0 Hz, 1H), 6.78−6.70 (m, 4H), 6.29−6.26 (m, 1H), 6.04 (br s, 1H), 5.25 (t, *J* = 5.0 Hz, 0.4H), 5.20 (d, *J* = 7.0 Hz, 0.4H), 5.06 (d, *J* =18.0 Hz, 0.4H), 4.98 (d, *J* =18.0 Hz, 0.6H), 4.90−4.87 (m, 0.6 H), 4.75−4.66 (m, 1.6H), 4.46−4.44 (m, 1H), 2.71−2.64 (m, 1H), 2.42−2.38 (m, 1H), 2.28−2.18 (m, 2H), 2.06−2.00 (m, 1H), 1.87−1.83 (m, 1H), 1.76−1.73 (m, 1H), 1.69−1.61 (m, 3H), 1.55−1.38 (m, 3H), 1.51 (s, 3H), 1.20−1.02 (m, 3H), 0.98−0.92 (m, 5H) ppm. *S*-**P10** and *R*-**P10** were obtained by chiral SFC separation of **P10**.

R-**P10**: ESI *m/z*: 522 (M + H)⁺; chiral SFC (CC4): 98.1 de%; ¹H NMR (400 MHz, CDCl₃) δ 7.23 (d, *J* = 10.1 Hz, 1H), 6.79 (dd, *J* = 8.8 Hz, 2H), 6.65 (d, *J* = 8.8 Hz, 2H), 6.27 (dd, *J* = 10.1, 1.7 Hz, 1H), 6.04 (s, 1H), 4.94 (d, *J* = 4.4 Hz, 1H), 4.89 (d, *J* = 18.0 Hz, 1H), 4.65 (d, *J* = 18.0 Hz, 1H), 4.61 (t, *J* = 4.4 Hz, 1H), 4.48 (d, *J* = 2.1 Hz, 1H), 3.51 (s, 2H), 2.58 (td, *J* = 13.3 Hz, 4.9 Hz, 1H), 2.35 (dd, *J* = 13.4 Hz, 2.8 Hz, 1H), 2.23−1.99 (m, 4H), 1.79−1.61 (m, 6H), 1.46−1.38 (m, 2H), 1.44 (s, 3H), 1.23−1.09 (m, 2H), 0.95 (s, 3H), 0.93 (t, *J* = 7.3 Hz, 3H) ppm.

S-**P10**: ESI *m/z*: 522 (M + H)⁺; chiral SFC (CC4): 99.5 de%; ¹H NMR (400 MHz, CDCl₃) δ 7.21 (d, *J* = 10.1 Hz, 1H), 6.77 (d, *J* = 8.8 Hz, 2H), 6.63 (d, *J* = 8.8 Hz, 2H), 6.24 (dd, *J* = 10.1, 1.6 Hz, 1H), 6.02 (s, 1H), 5.20 (d, *J* = 6.8 Hz, 1H), 5.18 (t, *J* = 4.8 Hz, 1H), 4.99 (d, *J* = -17.9 Hz, 1H), 4.61 (d, *J* = -17.9 Hz, 1H), 4.43 (s, 1H), 3.46 (s, 2H), 2.57 (td, *J* = 13.2 Hz, 4.4 Hz, 1H), 2.34 (dd, *J* = 13.4 Hz, 3.2 Hz, 1H), 2.16−2.01 (m, 4H), 1.85−1.68 (m, 3H), 1.59−1.49 (m, 3H), 1.44 (s, 3H), 1.44−1.26 (m, 2H), 1.18−1.09 (m, 2H), 1.00 (s, 3H), 0.91 (t, *J* = 7.3 Hz, 3H) ppm.

Synthesis of Payload P11 (Step vii in Scheme 1). Following general procedure of step vii, **P11** (9.0 mg, 44% yield) was obtained as a light orange solid after prep-HPLC purification (method A) from **IIB** (36 *μ*mol), 3-aminophenol (72 *μ*mol), and cesium carbonate (72 *μ*mol) in acetonitrile (0.5 mL). ESI *m/z*: 558 (M + H)⁺; ¹H NMR (500 MHz, CD₃OD) δ 7.35 (dd, *J* = 10.1, 1.3 Hz, 1H), 7.29 (t, *J* = 8.1 Hz, 1H), 6.76−6.70 (m, 3H), 6.40−6.29 (m, 2H), 5.66−5.48 (m, 1H), 5.14 (d, *J* = 18.1 Hz, 1H), 4.93−4.91 (m, 1H), 4.90−4.87 (m, 1H), 4.77 (t, *J* = 4.3 Hz, 1H), 4.35 (d, *J* = 9.3 Hz, 1H), 2.76−2.62 (m,

1H), 2.41−2.18 (m, 3H), 1.83−1.56 (m, 9H), 1.50 (dt, J = 15.4, 7.6 Hz, 2H), 0.99−0.96 (m, 6H) ppm.; *anal.* HPLC: purity is 100%.

Synthesis of Payloads P12, R-P12, and S-P12 (Step vii in Scheme 1). Following general procedure of step vii, **P12** (6.0 mg, 6.3%) was obtained as a white solid after prep-HPLC purification (method B) from **IIB** (0.17 mmol), 4-aminophenol (37 mg, 0.34 mmol), and cesium carbonate (0.11 g, 0.34 mmol) in acetone (0.5 mL). ESI m/z: 298 (M/2 + H)$^+$, 558 (M + H)$^+$ (10%); ^{1}H NMR (400 MHz, DMSO-d_6) δ 7.26 (d, J = 10.1 Hz, 1H), 6.67−6.65 (m, 2H), 6.52−6.48 (m, 2H), 6.30 (dd, J = 10.1, 1.8 Hz, 1H), 6.12 (s, 1H), 5.71−5.57 (m, 1H), 5.53−5.47 (m, 1H), 5.23 (t, J = 4.8 Hz, 0.2H), 5.15 (d, J = 7.2 Hz, 0.2H), 4.97 (m, 1H), 4.79 (m, 0.8H), 4.71−4.67 (m, 1H), 4.70−4.60 (m, 2.8H), 4.21 (m, 1H), 2.67−2.60 (m, 1H), 2.28−2.25 (m, 1H), 2.10−2.01 (m, 2H), 1.79−1.76 (m, 1H), 1.60−1.53 (m, 4H), 1.49 (s, 3H), 1.45−1.41 (m, 1H), 1.39−1.31 (m, 2H), 0.88 (t, J = 7.6 Hz, 3H), 0.83 (s, 3H) ppm.; *anal.* HPLC: purity is 97.4%. *S-*P12 and *R-*P12 were also obtained from chiral separation of **P12** or synthesized from enantio-pure starting materials using the same procedures.

*R-*P12: ESI m/z: 558 (M + H)$^+$; ^{1}H NMR (500 MHz, d_6-DMSO) δ 7.26 (d, J = 10.1 Hz, 1H), 6.64 (d, J = 8.8 Hz, 2H), 6.50 (d, J = 8.8 Hz, 2H), 6.30 (dd, J = 10.1, 1.8 Hz, 1H), 6.11 (s, 1H), 5.72−5.55 (m, 1H), 5.51 (d, J = 2.2 Hz, 1H), 4.97 (d, J = 18.4 Hz, 1H), 4.79 (m, 1H), 4.71−4.67 (m, 4H), 4.21 (m, 1H), 2.67−2.60 (m, 1H), 2.28−2.25 (m, 1H), 2.10−2.01 (m, 2H), 1.77 (d, J = 13.0 Hz, 1H), 1.60−1.52 (m, 4H), 1.49 (s, 3H), 1.45−1.41 (m, 1H), 1.39−1.31 (m, 2H), 0.87 (t, J = 7.4 Hz, 3H), 0.83 (s, 3H) ppm.; *anal.* HPLC: purity is 100%.

*S-*P12: ESI m/z: 558 (M + H)$^+$; ^{1}H NMR (400 MHz, d_6-DMSO) δ 7.27 (dd, J = 10.2, 1.0 Hz, 1H), 6.65−6.60 (m, 2H), 6.51−6.47 (m, 2H), 6.30 (dd, J = 10.2, 1.9 Hz, 1H), 6.11 (s, 1H), 5.71−5.67 (m, 1H), 5.52 (t, J = 4.9 Hz, 1H), 5.23 (t, J = 4.9 Hz, 1H), 5.15 (d, J = 7.2 Hz, 1H), 4.99 (d, J = 18.0 Hz, 1H), 4.69 (m, 2H), 4.63 (d, J = 18.0 Hz, 1H), 4.19 (m, 1H), 2.60−2.51 (m, 1H), 2.26−2.23 (m, 1H), 2.09−2.01 (m, 2H), 1.84−1.76 (m, 1H), 1.65−1.56 (m, 4H), 1.49 (s, 3H), 1.49−1.41 (m, 1H), 1.34−1.23 (m, 2H), 0.92−0.78 (m, 6H) ppm.; *anal.* HPLC: purity is >99%.

Synthesis of Payload P13 (Step vii in Scheme 1). Following the general procedure of step vii, a reaction of **IIB** (0.20 g, 0.36 mmol), *N*-Boc-4-aminomethylphenol (0.16 g, 0.72 mmol), and cesium carbonate (0.23 g, 0.72 mmol) in acetonitrile (4 mL) generated the Boc-intermediate of **P13** (0.20 g, 95% yield) as a brown oil after purification by flash chromatography (50% ethyl acetate in petroleum ether). ESI m/z: 594 (M + Na)$^+$. The Boc-intermediate of **P13** (30 mg, 45 μmol) was dissolved in CH$_2$Cl$_2$ (2 mL), cooled to 0 °C, and TFA (0.4 mL) was added dropwise. The resulting mixture was stirred at rt for 1 h. The volatiles were removed *in vacuo*, and the residue was purified by prep-HPLC (method A) to afford **P13** (15 mg, 49% yield) as a white solid. ESI m/z: 572 (M + H)$^+$; ^{1}H NMR (500 MHz, CD$_3$OD) δ 7.45−7.32 (m, 3H), 7.01−6.96 (m, 2H), 6.41−6.30 (m, 2H), 5.65−5.49 (m, 1H), 5.34−4.73 (m, 4H), 4.37−4.32 (m, 1H), 4.07 (s, 2H), 2.75−2.58 (m, 1H), 2.40−2.15 (m, 3H), 1.86−1.40 (m, 11H), 1.08−0.92 (m, 6H) ppm.; *anal.* HPLC: purity is 100%.

Synthesis of Payload P14 (Step vii in Scheme 1). Following general procedure of step vii, **P14** (90 mg, 70% yield) was obtained as a white solid from **IID** (0.16 g, 0.33 mmol), 4-nitrophenol, and cesium carbonate (0.80 mmol) in acetone (5 mL). ESI m/z: 502 (M + H)$^+$. ^{1}H NMR (500 MHz, d_6-DMSO) δ 7.27 (d, J = 10.2 Hz, 1H), 6.59 (d, J = 8.8 Hz, 2H), 6.49 (d, J = 8.8 Hz, 2H), 6.30 (dd, J = 10.1 Hz, 1.7 Hz, 1H), 6.11 (s, 1H), 5.75−5.54 (m, 1H), 5.42−5.39 (m, 1H), 5.22 (s, 1H), 5.07 (d, J = 18.3 Hz, 1H), 4.63 (s, 2H), 4.59 (d, J = 18.3 Hz, 1H), 4.18 (m, 1H), 2.99−2.91 (m, 1H), 2.55−2.43 (m, 1H), 2.25−2.19 (m, 3H), 1.71−1.64 (m, 1H), 1.56−1.43 (m, 5H), 1.15−1.10 (m, 1H), 0.88 (s, 3H), 0.83 (d, J = 6.0 Hz, 3H) ppm.; *anal.* HPLC: purity is 95%.

Synthesis of Linker−Payloads (LP1 and LP2 in Scheme 2). **LP1** and **LP2** were made in two steps from intermediates **VA** and **VB**, respectively. The first step was the synthesis of **VA** and **VB**. To a solution of **P3** (93 mg, 0.20 mmol) in DMF (30 mL) was added Fmoc-vcPAB-PNP (**IV**) (0.17 g, 0.22 mmol), hydroxybenzotriazole

(HOBT, 41 mg, 0.30 mmol), and DIPEA (52 mg, 0.40 mmol) at rt. The mixture was stirred at 18−30 °C for 3 h, and then piperidine (0.30 mL) was added and the mixture was stirred at 18−30 °C for 1 h. The reaction mixture was filtered and purified by reversed-phase flash chromatography (50−80% acetonitrile in aq. ammonium bicarbonate (10 mM)) to give compound **VA** as a white solid (0.13 g, 73% yield). ESI m/z: 871 (M + H)$^+$; ^{1}H NMR (400 MHz, DMSO-d_6) δ 10.13 (s, 1H), 8.18−8.10 (m, 1H), 7.60 (d, J = 8.4 Hz, 2H), 7.43 (t, J = 5.8 Hz, 1H), 7.30 (d, J = 8.5 Hz, 2H), 7.27 (d, J = 10.1 Hz, 1H), 6.31 (dd, J = 10.1, 1.5 Hz, 1H), 6.11 (s, 1H), 5.98 (t, J = 5.3 Hz, 1H), 5.74−5.54 (m, 2H), 5.41 (s, 2H), 4.98 (s, 2H), 4.82−4.72 (m, 1H), 4.59 (t, J = 4.1 Hz, 1H), 4.52−4.43 (m, 1H), 4.33−4.08 (m, 2H), 3.90−3.77 (m, 1H), 3.11−2.88 (m, 3H), 2.71−2.53 (m, 1H), 2.34−2.19 (m, 1H), 2.12−1.88 (m, 4H), 1.82−1.53 (m, 7H), 1.49 (s, 3H), 1.46−1.27 (m, 5H), 0.96−0.72 (m, 13H) ppm. By using the same method as above, **VB** was obtained as a white solid (80 mg, 64% yield) from **P12** (87 mg, 0.15 mmol). ESI m/z: 963 (M + H)$^+$; ^{1}H NMR (500 MHz, d_6-DMSO) δ 10.22 (s, 1H), 9.57 (s, 1H), 8.69 (d, J = 7.5 Hz, 1H), 8.08 (s, 3H), 7.61 (d, J = 6.8 Hz, 2H), 7.36 (d, J = 6.8 Hz, 3H), 7.27 (d, J = 8.0 Hz, 1H), 7.22−7.0 (m, 1H), 6.84 (d, J = 7.2 Hz, 2H), 6.30 (dd, J = 8.0 Hz, J = 1.6 Hz, 1H), 6.11 (s, 1H), 6.10−6.0 (m, 1H), 5.72−5.55 (m, 1H), 5.52 (s, 1H), 5.48 (s, 1H), 5.16−5.05 (m, 3H), 4.88−4.80 (m, 1H), 4.80−4.76 (m, 1H), 4.75−4.70 (m, 1H), 4.55−4.48 (m, 1H), 4.25−4.20 (m, 1H), 3.70−3.60 (m, 1H), 3.12−2.90 (m, 2H), 2.70−2.55 (m, 1H), 2.40−2.20 (m, 1H), 2.15−2.0 (m, 3H), 1.86−1.75 (m, 1H), 1.75−1.65 (m, 1H), 1.64−1.54 (m, 5H), 1.49 (s, 4H), 1.46−1.34 (m, 4H), 0.97−0.91 (m,5H), 0.90−0.85 (m, 4H), 0.85−0.80 (m, 3H) ppm.

The second step is the synthesis of **LP1** and **LP2** from **VA** and **VB**, respectively. To a solution of DIBAC-suc-PEG$_4$-acid (**VI**, 33 mg, 60 μmol) in DMF (3 mL) were added HATU (25 mg, 66 μmol) and DIPEA (32 mg, 0.25 mmol) at rt. The mixture was stirred for 30 min followed by the addition of a solution of **VA** or **VB** (43 mg, 50 μmol) in DMF (2.5 mL). The resulting mixture was stirred at rt for 2 h, filtered, and purified by prep-HPLC (5−95% acetonitrile in aq. ammonium bicarbonate (10 mM)) to give **LP1** (16 mg, 23% yield) or **LP2** (20 mg, 22% yield) as white solids. For **LP1**, ESI m/z: 1406 (M + H)$^+$; ^{1}H NMR (d_6-DMSO, 500 MHz) δ 9.99 (s, 1H), 8.11 (d, J = 7.5 Hz, 1H), 7.88 (d, J = 8.5 Hz, 1H), 7.80−7.75 (m, 1H), 7.70−7.66 (m, 1H), 7.65−7.60 (m, 3H), 7.53−7.33 (m, 6H), 7.33−7.28 (m, 3H), 6.30 (dd, J = 10.0 and 1.5 Hz, 1H), 6.11 (s, 1H), 6.10−6.00 (m, 1H), 5.72−5.55 (m, 2H), 5.41 (s, 2H), 5.05−5.01 (m, 1H), 4.97 (s, 2H), 4.80−4.72 (m, 1H), 4.60−4.58 (m, 1H), 4.43−4.33 (m, 1H), 4.25−4.10 (m, 3H), 3.88−3.80 (m, 1H), 3.65−3.55 (m, 3H), 3.50−3.40 (m, 12H), 3.30−3.25 (m, 2H), 3.12−2.90 (m, 4H), 2.70−2.55 (m, 2H), 2.48−2.35 (m, 2H), 2.30−2.20 (m, 2H), 2.15−1.95 (m, 4H), 1.86−1.65 (m, 3H), 1.64−1.54 (m, 5H), 1.49 (s, 4H), 1.46−1.34 (m, 5H), 0.90−0.80 (m, 12H) ppm.; *anal.* HPLC: 100%. For **LP2**, ESI m/z: 1499 (M + H)$^+$; ^{1}H NMR (400 MHz, d_6-DMSO) δ 10.02 (s, 1H), 9.59 (s, 1H),8.14 (d, J = 7.6 Hz, 1H), 7.88 (d, J = 8.8 Hz, 1H), 7.80−7.75 (m, 1H), 7.70−7.66 (m, 1H), 7.65−7.60 (m, 3H), 7.53−7.45 (m, 3H), 7.40−7.28 (m, 7H), 6.84 (d, J = 9.2 Hz, 2H), 6.30 (dd, J = 10.4 Hz, J = 1.6 Hz, 1H), 6.11 (s, 1H), 6.10−6.0 (m, 1H), 5.72−5.55 (m,1H), 5.52 (s, 1H), 5.43 (s, 2H), 5.16−5.05 (m, 4H), 4.88−4.70 (m, 3H), 4.43−4.33 (m, 1H), 4.25−4.20 (m, 2H), 3.65−3.55 (m, 3H), 3.50−3.40 (m, 12H), 3.30−3.25 (m, 2H), 3.12−2.90 (m, 4H), 2.70−2.55 (m, 2H), 2.48−2.43 (m, 1H), 2.40−2.35 (m, 1H), 2.30−2.20 (m, 2H), 2.15−1.95 (m, 4H), 1.86−1.75 (m, 2H), 1.64−1.54 (m, 5H), 1.49 (s, 4H), 1.46−1.34 (m, 4H), 1.23 (s, 2H), 0.90−0.80 (m, 12H) ppm.; *anal.* HPLC: purity is 100%.

Synthesis of Quenched Linker−Payload (q-LP1 and q-LP2 in Scheme 2). The quenched linker−payloads (**q-LP1** and **q-LP2**) were prepared from **LP1** and **LP2**, respectively, via a strain-promoted azide−alkyne cycloaddition (SPAAC) reaction between **LP1** or **LP2** with azido−PEG$_4$−SO$_3$H (**VIII**). The building block azido−PEG$_4$− SO$_3$H (**VIII**) was prepared from commercial reagent **VII**. To a solution of **VII** (0.58 g, 1.5 mmol) in DMF (10 mL) were added taurine (0.23 g, 1.8 mmol) and DIEA (0.58 g, 4.5 mmol). The reaction mixture was stirred at rt for 18 h. The resulting mixture was directly purified by prep-HPLC (method A) to give **VIII** (0.56 g, 94%

yield) as a colorless oil. ESI m/z: 399 $(M + H)^+$. To a solution of **LP1** (5.9 mg, 4.2 μmol) in acetonitrile (0.5 mL) was added a solution of **VIII** (8.4 mg, 21 μmol) in water (0.5 mL). The mixture was stirred at rt for 18 h and was then directly purified by prep-HPLC (method B) to give **q-LP1** (3.8 mg, 50% yield) as a white solid. ESI m/z: 902.5 $(M/2 + H)^+$; *anal.* HPLC: purity is >99%, R_t 7.16 min. Using the same procedures as described above, **q-LP2** (6.5 mg, 51% yield) was obtained as a white solid from **LP2** (10 mg, 6.7 μmol) and **VIII** (5.0 mg, 13 μmol). ESI m/z: 949 $(M/2 + H)^+$; *anal.* HPLC: purity is 96%, R_t 7.14 min.

*Conjugation of Azido-Functionalized Antibody (**Ab−N₃** in Scheme 3).* Aglycosylated antibody with a human IgG1 isotype was mixed with a solution of azido−PEG₃−amine (200 mol equiv to the antibody, F.W. 218.26) in BupH, and the solution was adjusted to pH 7.0−7.4 with conc. HCl. Transglutaminase (5U MTG per mg of antibody obtained either from Zedira, Darmstadt, Germany, or ACTIVA TI from Ajinomoto) in PBS buffer was added to obtain a final concentration of the antibody of 0.5−10 mg/mL. The solution was incubated at 37 °C for 4−24 h, while gently shaking, and the progress of the reaction was monitored by ESI-MS until the parental antibody was consumed. The excess amine and MTG were removed by size exclusion chromatography (SEC) to generate the site-specific antibody−azide conjugate (**Ab−N₃**).

Site-Specific Antibody−Drug Conjugates via Click Chemistry Reactions (in Scheme 3). A site-specific antibody conjugate with linker−payload **LP1** or **LP2** was prepared by incubating **Ab−N₃** (1−10 mg/mL) in PBS (pH 7.4) with >6 molar equivalents of **LP1** or **LP2** in DMSO, DMF, or *N,N*-dimethylacetamide (DMA) at a concentration of 10 mg/mL, resulting in the reaction mixture containing ~5−20% organic solvent (v/v). The mixture was stirred at 24−37 °C for 1−6 h. The progress of the reaction was monitored by ESI-MS, and the absence of **Ab−N₃** indicated the completion of the conjugation. The excess amount of **LP1** or **LP2** and organic solvent were removed by SEC (Superdex 200 HR, GE Healthcare) in PBS buffer. The purified conjugates were concentrated by ultracentrifugation and characterized by SEC, sodium dodecyl sulfate polyacrylamide gel electrophoresis (SDS-PAGE), and ESI-LC-MS.

■ ASSOCIATED CONTENT

Ⓢ Supporting Information

The Supporting Information is available free of charge at https://pubs.acs.org/doi/10.1021/acs.jmedchem.1c00541.

Compounds P1−P14, SMILES (CSV)
Figure 2A (PDB)
Figure 2B (PDB)
Figure S2 (PDB)
Figure S3 (PDB)
Figure S4a (PDB)
Figure S4b (PDB)
Figure S5 (PDB)
Figure S6 (PDB)
Supporting information describes further detail for (1) modeling of GCs in complexes with glucocorticoid receptor (GR) and the 3D modeling results in PBD files; (2) separation of chiral GCs by SFC and HPLC and structural determination of chiral GCs by NOESY and NMR, as well as LC-MS traces and SMILE formula strings of all compounds, (3) ESI-MS spectra of site-specific ADCs, (4) *in vitro* bioassays of cell-free GR binding and cell-free nuclear receptor (NR) binding assay panels, cell-based reporter assay, and Bystander effect assay, (5) ADME assays including plasma stability, Caco2, and cathepsin B enzymatic assay, (6) *in vivo* LPS-induced TNFα release model, (7) pharmacokinetic data of P3 and P12, and (8) structures with SMILE formula strings (PDF)

■ AUTHOR INFORMATION

Corresponding Author

Amy Han − *Regeneron Pharmaceuticals, Inc., Tarrytown, New York 10591, United States;* ⓘ orcid.org/0000-0001-5012-8262; Email: amy.han@regeneron.com

Authors

Olav Olsen − *Regeneron Pharmaceuticals, Inc., Tarrytown, New York 10591, United States*

Christopher D'Souza − *Regeneron Pharmaceuticals, Inc., Tarrytown, New York 10591, United States*

Jing Shan − *Regeneron Pharmaceuticals, Inc., Tarrytown, New York 10591, United States*

Feng Zhao − *Regeneron Pharmaceuticals, Inc., Tarrytown, New York 10591, United States*

Jean Yanolatos − *Regeneron Pharmaceuticals, Inc., Tarrytown, New York 10591, United States*

Zaruhi Hovhannisyan − *Regeneron Pharmaceuticals, Inc., Tarrytown, New York 10591, United States*

Sokol Haxhinasto − *Regeneron Pharmaceuticals, Inc., Tarrytown, New York 10591, United States*

Frank Delfino − *Regeneron Pharmaceuticals, Inc., Tarrytown, New York 10591, United States*

William Olson − *Regeneron Pharmaceuticals, Inc., Tarrytown, New York 10591, United States*

Complete contact information is available at:
https://pubs.acs.org/10.1021/acs.jmedchem.1c00541

Notes

The authors declare no competing financial interest.

■ KEY ABBREVIATIONS

ADC, antibody−drug conjugate; DAR, drug-to-antibody ratio; GC, glucocorticoids; GR, glucocorticoid receptor; LP, linker-payloads; MTG, microbial transglutaminase; vcPAB, L-valine-L-citrulline-*p*-aminobenzyl alcohol

■ REFERENCES

(1) Berlin, M. Recent advances in the development of novel glucocorticoid receptor modulators. *Expert Opin. Ther. Pat.* **2010**, *20*, 855−873.

(2) Chang, S.; Hanauer, S. Optimizing pharmacologic management of inflammatory bowel disease. *Expert Rev. Clin. Pharmacol.* **2017**, *10*, 595−607.

(3) Ford, A.; Bernstein, C.; Khan, K.; Abreu, M.; Marshall, J. K.; Talley, N. J.; Moayyedi, P. Glucocorticosteroid therapy in inflammatory bowel disease: systematic review and meta-analysis. *Am. J. Gastroenterol.* **2011**, *106*, 590−599.

(4) Chikanza, I. Mechanisms of corticosteroid resistance in rheumatoid arthritis: a putative role for the corticosteroid receptor β isoform. *Ann. N. Y. Acad. Sci.* **2002**, *966*, 39−48.

(5) Dubois-Camacho, K.; Ottum, P.; Franco-Muñoz, D.; Fuente, M. D.; Torres-Riquelme, A.; Díaz-Jiménez, D.; Olivares-Morales, M.; et al. Glucocorticosteroid therapy in inflammatory bowel diseases: From clinical practice to molecular biology. *World J. Gastroenterol.* **2017**, *23*, 6628−6638.

(6) ClinicalTrials.gov Identifier: NCT03823391.

(7) Brandish, P. E.; Palmieri, A.; Antonenko, S.; Beaumont, M.; Benso, L.; Cancilla, M.; Cheng, M.; Fayadat-Dilman, L.; Feng, G.;

Figueroa, I.; Firdos, J.; Garbaccio, R. M.; Garvin-Queen, L.; Gately, D.; Geda, P.; Haines, C.; Hseih, H. D.; Kern, J.; Knudsen, N.; Kwasnjuk, K.; Liang, L.; Ma, H.; Manibusan, A.; Miller, P.; Moy, L.; Qu, Y.; Shah, D.; Shin, J.; Stivers, P.; Sun, Y.; Tomazela, D.; Woo, H. C.; Zaller, D.; Zhang, S.; Zhang, Y.; Zielstorff, M.; et al. Development of anti-CD74 antibody−drug conjugates to target glucocorticoids to immune cells. *Bioconjugate Chem.* **2018**, *29*, 2357−2369.

(8) Kern, J. C.; Dooney, D.; Zhang, R.; Liang, L.; Brandish, P. E.; Cheng, M.; Feng, G.; Beck, A.; Bresson, D.; Firdos, J.; Gately, D.; Knudsen, N.; Manibusan, A.; Sun, Y.; Garbaccio, R. M. Novel phosphate modified cathepsin B linkers: improving aqueous solubility and enhancing payload scope of ADCs. *Bioconjugate Chem.* **2016**, *27*, 2081−2088.

(9) Han, A.; Murphy, A.; Olson, W. Steroids and protein-conjugates thereof. US Patent 15/860,197, June 7, 2018.

(10) Pishesha, N.; Harmand, T.; Smeding, L.; Ma, W.; Ludwig, L.; Janssenv, R.; Islam, A.; Xie, Y.; Feng, T.; McCaul, N.; Pinney, W.; Sugito, H.; Ploegh, H. Single domain antibody-antigen adducts that target class II MHC induce antigen-specific tolerance. DOI: 10.21203/rs.3.rs-192181.

(11) Edman, K.; Hosseini, A.; Bjursell, M.; Aagaard, A.; Wissler, L.; Gunnarsson, A.; Kaminski, T.; Köhler, C.; Bäckström, S.; Jensen, T.; Cavallin, A.; Karlsson, U.; Nilsson, E.; Lecina, D.; Takahashi, R.; Grebner, C.; Geschwindner, S.; Lepistö, M.; Hogner, A.; Guallar, V. Ligand binding mechanism in steroid receptors: from conserved plasticity to differential evolutionary constraints. *Structure* **2015**, *23*, 2280−2290.

(12) Angell, R. M.; Biggadike, K.; Farrell, R.; Flack, S.; Hancock, A. P.; Irving, W.; Lynna, S. M.; Procopiou, P. Novel glucocorticoid antedrugs possessing a 21-(γ-lactone) ring. *J. Chem. Soc., Perkin Trans. 1* **2002**, *6*, 831−839.

(13) Biju, P.; Bitar, R.; Lim, Y. H.; Wang, Y.; Berlin, M.; Aslanian, R.; McCormick, K. Synthesis of novel anti-inflammatory steroidal macrocycles using ring closing metathesis reaction. *Tetrahedron Lett.* **2015**, *56*, 636−638.

(14) Thalen, A. Epimers of budesonide and related corticosteroids. III. synthesis and structure elucidation by carbon-13 and proton nuclear magnetic resonance spectroscopy. *Acta Pharm. Suec.* **1987**, *24*, 97−114.

(15) Wang, Z.; Hop, C.; Leung, K. H.; Pang, J. Determination of in vitro permeability of drug candidates through a Caco-2 cell monolayer by liquid chromatography/tandem mass spectrometry. *J. Mass. Spec.* **2000**, *35*, 71−76.

(16) Brattsand, R.; Thalén, A.; Roempke, K.; Källström, L.; Gruvstad, E. Influence of 16α,17α-acetal substitution and steroid nucleus fluorination on the topical to systemic activity ratio of glucocorticoids. *J. Steroid Chem.* **1982**, *16*, 779−786.

(17) Procopiou, P. A.; Biggadike, K.; English, A. F.; Farrell, R. M.; Hagger, G. N.; Hancock, A. P.; Haase, M. V.; Irving, W. R.; Sareen, M.; Snowden, M. A.; Solanke, Y. E.; Tralau-Stewart, C. J.; Walton, S. E.; Wood, J. A. Novel glucocorticoid antedrugs possessing a 17β-(γ-lactone) Ring. *J. Med. Chem.* **2001**, *44*, 602−612.

(18) Held, F.; Hoppe, E.; Cvijovic, M.; Jirstrand, M.; Gabrielsson, J. Challenge model of TNFα turnover at varying LPS and drug. *J. Pharmacokinet. Pharmacodyn.* **2019**, *46*, 223−240.

(19) Danker, T.; Moller, C. Early identification of hERG liability in drug discovery programs by automated patch clamp. *Front. Pharmacol.* **2014**, *5*, 203.

(20) Maron, D. M.; Ames, B. N. Revised methods for the salmonella mutagenicity test. *Mutat. Res., Environ. Mutagen. Relat. Subj.* **1983**, *113*, 173−215.

(21) Caculitan, N. G.; Chuh, J.; Ma, Y.; Zhang, D.; Kozak, K. R.; Liu, Y.; Pillow, T. H.; Sadowsky, J.; Cheung, T. K.; Phung, Q.; Haley, B.; Lee, B. C.; Akita, R. W.; Sliwkowski, M. X.; Polson, A. G. Cathepsin B is dispensable for cellular processing of cathepsin B-cleavable antibody-drug conjugates. *Cancer Res.* **2017**, *77*, 7027−7037.

(22) Jain, N.; Smith, S. W.; Ghone, S.; Tomczuk, B. Current ADC linker chemistry. *Pharm. Res.* **2015**, *32*, 3526−3540.

(23) Han, A.; Olson, W. Optimized transglutaminase site-specific antibody conjugation. WO2017147542A3.

(24) Kelly, M.; Hickey, C.; Makonnen, S.; Coetzee, S.; Jalal, S.; Wang, Y.; Delfino, F.; Shan, J.; Potocky, T.; Chatterjee, I.; Andreev, J.; Kunz, A.; D'Souza, C.; Giurleo, J.; Nittoli, T.; Trail, P.; Thurston, G.; Kirshner, J. Preclinical activity of the novel anti-prolactin receptor (PRLR) antibody-drug conjugate REGN2878-DM1 in PRLR-positive breast cancers. *Mol. Cancer Ther.* **2017**, *16*, 1299−1311.

(25) Kleine-Tebbe, J.; Kleine-Tebbe, A.; Jeep, S.; Schou, C.; Lowenstein, H.; Kunkel, G. Role of the major allegen (Fel d1) in patients sensitized to cat allergens. *Int. Arch. Allergy Immunol.* **1993**, *100*, 256−262.

(26) *Schrödinger Release 2017-3: Schrodinger discovery suite paper*; Schrödinger, LLC: New York, NY, 2017.

(27) (A) Strop, P.; Liu, S. H.; Dorywalska, M.; Delaria, K.; Dushin, R. G.; Tran, T. T.; Ho, W. H.; Farias, S.; Casas, M. G.; Abdiche, Y.; Zhou, D.; Chandrasekaran, R.; Samain, C.; Loo, C.; Rossi, A.; Rickert, M.; Krimm, S.; Wong, T.; Chin, S. M.; Yu, J.; Dilley, J.; Chaparro-Riggers, J.; Filzen, G. F.; O'Donnell, C. J.; Wang, F.; Myers, J. S.; Pons, J.; Shelton, D. L.; Rajpal, A. Location matters: site of conjugation modulates stability and pharmacokinetics of antibody drug conjugates. *Chem. Biol.* **2013**, *20*, 161−167. (B) Dickgiesser, S.; Rieker, M.; Mueller-Pompalla, D.; Schröter, C.; Tonillo, J.; Warszawski, S.; Raab-Westphal, S.; Kühn, S.; Knehans, T.; Könning, D.; Dotterweich, J.; Betz, U.; Anderl, J.; Hecht, S.; Rasche, N. Site-specific conjugation of native antibodies using engineered microbial transglutaminases. *Bioconjugate Chem.* **2020**, *31*, 1070−1076. (C) Hussain, A. F.; Grimm, A.; Sheng, W.; Zhang, C.; Al-Rawe, M.; Bräutigam, K.; Mraheil, M. A.; Zeppernick, F.; Heerlein, I. M. Toward homogenous antibody drug conjugates using enzyme-based conjugation approaches. *Pharmaceuticals* **2021**, *14*, 343. (D) Anami, Y.; Tsuchikama, K. Transglutaminase-Mediated Conjugations. In *Methods in Molecular Biology*; Humana: New York, 2020; Vol. *2078*, pp 71−82. (E) Miller, J. T.; Vitro, C. N.; Fang, S.; Benjamin, S. R.; Tumey, L. N. Enzyme-agnostic lysosomal screen identifies new legumain-cleavable ADC linkers. *Bioconjugate Chem.* **2021**, *32*, 842−858.